

Topology Optimization with Accessibility Constraint for Multi-Axis Machining

Amir M. Mirzendehtdel, Morad Behandish, and Saigopal Nelaturi

Palo Alto Research Center (PARC), 3333 Coyote Hill Road, Palo Alto, California 94304

Abstract

In this paper, we present a topology optimization (TO) framework to enable automated design of mechanical components while ensuring the result can be manufactured using multi-axis machining. Although TO improves the part's performance, the as-designed model is often geometrically too complex to be machined and the as-manufactured model can significantly vary due to machining constraints that are not accounted for during TO. In other words, many of the optimized design features cannot be accessed by a machine tool without colliding with the part (or fixtures). The subsequent post-processing to make the part machinable with the given setup requires trial-and-error without guarantees on preserving the optimized performance. Our proposed approach is based on the well-established accessibility analysis formulation using convolutions in configuration space that is extensively used in spatial planning and robotics. We define an *inaccessibility measure field* (IMF) over the design domain to identify non-manufacturable features and quantify their contribution to non-manufacturability. The IMF is used to penalize the sensitivity field of performance objectives and constraints to prevent formation of inaccessible regions. Unlike existing discrete formulations, our IMF provides a continuous spatial field that is desirable for TO convergence. Our approach applies to arbitrary geometric complexity of the part, tools, and fixtures, and is highly parallelizable on multi-core architecture. We demonstrate the effectiveness of our framework on benchmark and realistic examples in 2D and 3D. We also show that it is possible to directly construct manufacturing plans for the optimized designs based on the accessibility information.

Keywords: Design for Manufacturing, Topology Optimization, Accessibility Analysis, Multi-Axis Machining, CNC Machining, Configuration Space, Hybrid Manufacturing

1. Introduction

Recent advances in computation and manufacturing technologies have enabled engineers to improve quality, increase productivity, and reduce cost by automating various stages of design and production. However, in many cases the discrepancies between as-design and as-manufactured models can result in excessive trial-and-error cycles or even render the design completely non-manufacturable. Incorporating manufacturing constraints early on during the design stage is essential for successful automation of computational design workflows.

Topology optimization (TO) [1, 2] is a computational tool for automated design that enables engineers across multiple disciplines ranging from biomedical [3] to automotive [4] and aerospace [5] explore the expansive design space of functional components. The interest in TO stems from recent advances in computational capabilities, new materials, and manufacturing technologies, where multi-functional components can be optimized with high fidelity to generate complex “organic” shapes that reduce cost while improving performance. Advances in additive manufacturing (AM) have enabled engineers to produce complex geometries designed by TO. However, many industrial parts require high precision and surface quality that, as of today, can only be achieved by subtractive manufacturing (SM) technologies such as multi-axis machining. Cur-

rent advances in automated manufacturing technologies have also enabled hybrid manufacturing (HM) processes that combine the complementary capabilities of AM and SM to achieve customization, cost-effectiveness, geometric complexity, precision, and surface quality for industrial functionality [6–9].

The focus of this paper is on developing a TO framework based on sound mathematical concepts from spatial planning [10] to incorporate multi-axis machining constraints early on during the design stage. The present work will substantially reduce the time and resources spent on post-optimization trial-and-error by bridging the gap between design and a widely used set of manufacturing processes. We will demonstrate the effectiveness of our proposed framework by considering realistic examples for 3- and 5-axis milling setups as shown in Fig. 1. Our method relies on a quantification of inaccessibility by any combination of translational and rotational degrees of freedom (DOF) as a continuous spatial field (called IMF) in 3D, which can be rapidly computed in parallel for intermediate designs of arbitrary geometric and topological complexities generated by TO.

In the remainder of this section, we review recent advances in design for manufacturing (DfM)—with a focus on incorporating manufacturability considerations into TO—and accessibility analysis (Section 1.1). We then present the contributions and outline of the paper (Section 1.3).

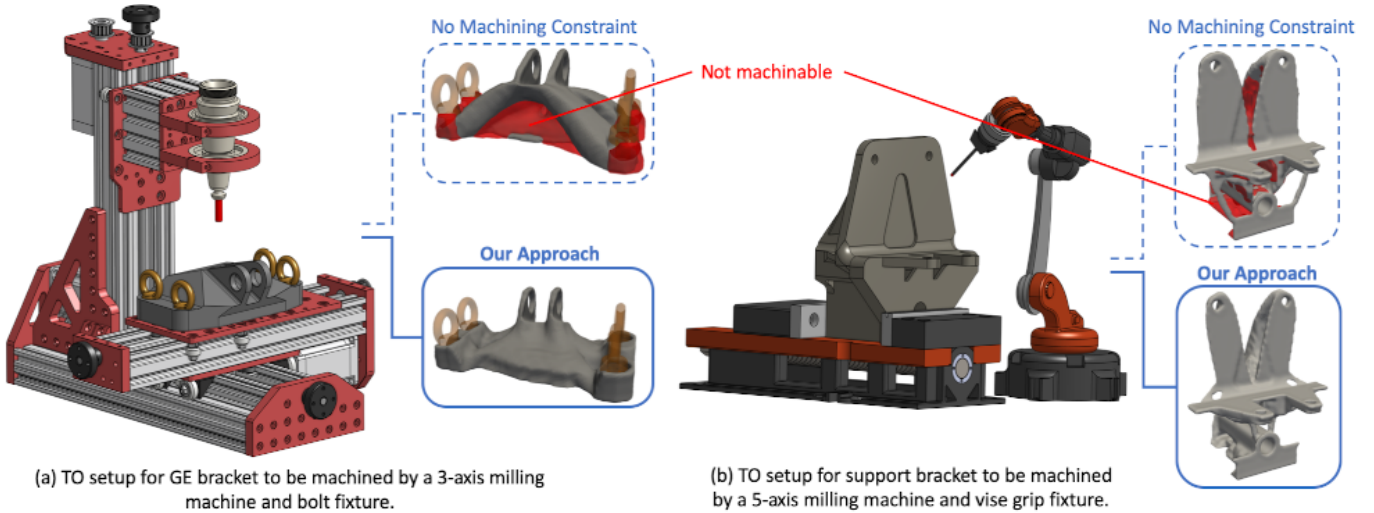


Figure 1: This article presents a generic approach to incorporate accessibility constraints for multi-axis machining into the design optimization process. The inputs are the shapes of initial design (e.g., the brackets shown above), stationary obstacles such as fixtures, moving objects including the entire tool assembly, and the available orientations. The output is an optimized design that is guaranteed to be accessible everywhere in the negative space of the part in at least one configuration and the set of all such configurations at the desired sampling resolution. The examples are demonstrative of arbitrary geometric complexity, and do not correspond to real industrial setups.

1.1. Related Work

The literature on TO with manufacturability constraints is broad, and our brief overview of the most relevant works in this section is by no means comprehensive. More detailed surveys can be found in [11–14].

With the growing interest in AM processes, design for additive manufacturing (DfAM) has emerged as an important paradigm to include AM constraints in early stages of design. These constraints pertain to minimum feature size [15], efficient use of support structure [16–18], anisotropic material properties [19, 20], and post-processing [13, 21].

For traditional manufacturing processes, DfM-based TO has mainly focused on minimum feature size, casting, linear and axial symmetry, and wire-cut for 2.5D structures. For casting and profile milling, the final design is constrained to have no undercuts or cavities along a prescribed draw/mill direction. A number of approaches have been used such as filtering of density fields [22], filtering of sensitivity fields [23], projecting parametric design variables onto element density spaces [24, 25], and imposing limits on the maximum of a virtual temperature field [26].

For machining with few DOF (e.g., 2.5D profiling), the range of solutions for TO can be restricted in terms of manufacturable “features” of shape. For instance, a feature-based shape optimization was proposed in [27] by incorporating a feature-fitting algorithm into levelset TO. The feature-based TO was extended to include a limited set of hybrid (combined AM/SM) manufacturing constraints for 2.5D profiling [28] and overhang-free 3D printing [29]. Unfortunately, feature-based modeling presents several ambiguities for process planning that prevent scalability with increasing geometric complexity. Increasing the DOF adds to the complexity of defining and identifying features for intermediate designs generated by TO.

Projection methods, on the other hand, are particularly suitable for designing modular layouts as in structures constructed by joining (e.g., welding) parameterized primitives such as bars or plates [30, 31]. A unified projection-based scheme was developed in [25] to consider various constraints including minimum member size, minimum hole size, symmetry, pattern repetition, extrusion, turning, casting, forging, and rolling by applying different variable mapping rules. Recently, a TO framework for 5-axis machining was proposed in [32], where the sensitivity field is filtered by accumulation of densities along tool insertion directions for a given set of simple prismatic tool shapes, insertion depths, and directions. It demonstrates that coupling morphological operations with projection methods is an effective approach to enforce machining constraints in TO. However, the assumption that the tool can approach the part only along straight line paths can over-constrain the TO with complex tool shapes and motion DOF.

A common limitation of feature-based or projection-based approaches is that a wide range of nontrivial designs with freeform features that can only be fabricated by complex tool shapes and motions might be excluded from the design space parameterization. Moreover, they do not rigorously formulate collision avoidance between the stationary objects (i.e., workpiece and fixtures) and moving objects (i.e., entire tool assembly). To realize the full potential and flexibility of TO in generating non-parametric shapes, there is a need for a more generic mathematical formulation of accessibility that 1) applies to candidate designs of arbitrary shape, not necessarily modeled via feature taxonomies or projected from predefined geometric building blocks; 2) provides a continuous quantification of inaccessibility to guide gradient/sensitivity-based TO; and 3) can be computed rapidly within a TO loop.

Accessibility and collision avoidance have been extensively studied in spatial planning and robotics [10, 33]. The notion of a configuration space (C-space) of relative 6D motions, i.e., group of rigid-body translations and rotations, is introduced to abstract collision predicates between two arbitrary 3D rigid bodies in relative motion to a point membership query against a 6D pointset, referred to as the configuration space obstacle (C-obstacle). Computing C-obstacles for arbitrary shapes can be challenging, depending on the choice of representation. For 5-axis machining applications, one of the six DOF for rotation around the tool axis is deemed redundant and the problem is simplified by assuming simple shapes for the rotating tool’s closure such as a flat/ball-end cylinders, approximating reachability by visibility, and so on [34–41]. However, the computations can be dramatically simplified by sampling-based approximations [42]. It has been shown that collision measures can be obtained as convolutions of indicator functions of the two bodies [43], and computed rapidly via fast Fourier transform (FFT) if these functions are sampled over uniform grids (i.e., voxelization) [44]. The convolution field provides an implicit representation of the C-obstacle as its 0–superlevel set. Moreover, the field value provides a measure of collision that quantifies inaccessibility and varies continuously with motion. In this paper, we show how this 6D field can be projected back to 3D to be used as a penalty function for TO.

In a recent article [45], we presented a formal definition of inaccessibility measure that is well-suited for TO. The proposed measure is agnostic to geometric complexities of part, tool assembly, and surrounding fixtures, as well as the motion DOF. However, its effectiveness was demonstrated only for simple 2D examples in [45] using a Pareto tracing levelset TO [46]. In this paper, we generalize the inaccessibility measure and extend its implementation to 3D for density-based TO, and demonstrate its effectiveness by optimized non-parametric designs with manufacturability guarantees for high-axis CNC machining with arbitrary fixture and tool assembly shapes and cutting orientations. To the best of our knowledge, none of the published TO frameworks provide matching extensive flexibilities.

1.2. A Note on Constraint Classification

The accessibility constraint is typically classified as a ‘set constraint’ and is expressed in the language of set containment, interference, affine transformations, and Boolean operations rather than the more commonly used real-valued functions that appear in (in)equality constraints for TO (e.g., bounds on stress or deformation) and other conventional constrained optimization problem formulations. To properly formulate the optimization problem by simultaneously considering set constraints for manufacturing and (in)equality constraints for performance, we rely on the classification scheme presented in [45]. We classify the constraints as global, local, and strictly local (i.e., pointwise) constraints.

Global constraints are evaluated in terms of a real-valued property over the entire design, such as compliance or p-norm of stress. Local constraints are evaluated at each point of the design but are also dependent on membership of other points in the design. Although they can also be interpreted as global constraints, there are advantages to local formulation (i.e., as a field in 3D) for TO. Accessibility constraint falls under this category, as collisions occurring anywhere in the design, possibly far from a given query point, affects deciding and quantifying the (in)accessibility of that point. Finally, strictly local (or pointwise) constraints can be evaluated at every point of the design without any knowledge of the membership of other points in the design. Accessibility constraint becomes pointwise only when the motion is independent of the global shape, e.g., if the collisions can only occur between the tool and fixtures, regardless of the workpiece’s evolving shape. See [45] (Section 4.4) for an example with 2.5D wire-/laser-cutting of a sheet material. Pointwise constraints directly lead to the definition of a point membership classification (PMC) for a maximal pointset that represents the entire feasible design subspace of the constraint, hence is used to ‘prune’ the design space prior to optimization. In this paper, we are interested in the more complex case of high-axis motions in which this assumption is invalid and the part’s own shape plays an important role in quantifying (in)accessibility.

Global constraints are widely used in TO and are typically expressed as a differentiable functional, for which a continuous sensitivity field can be computed at every point in the 3D design domain. We showed in [45] that local constraints can be directly incorporated into the sensitivity field as a penalty. However, if the penalty function is not continuous, the resulting discontinuities in the “augmented” sensitivity field can adversely affect the convergence of TO to useful designs. Although the set constraint for accessibility can be easily converted to an (in)equality constraint in terms of discontinuous indicator functions (e.g., 1 for inaccessible points and 0 for accessible points) or a continuous field in 6D (e.g., the convolution), it is not trivial to define it as a continuous field in the 3D space for motions with arbitrary rotational DOF in multi-axis machining. For small tools and purely translational motions, an approximation to IMF can be obtained by establishing a simple one-to-one correspondence between the translation C-space and 3D design domain by selecting a representative point on the cutter. Every point in the design domain is assigned the value of convolution corresponding to the collision measure for the translation that takes the representative point to the query point. In [45], we demonstrated that the resulting field makes for an effective penalty for filtering the sensitivity field for producing manufacturable designs in simple 2D examples with small 2D tools at a few orientations. In this paper, we present a generic definition of IMF that is usable for arbitrary shapes in 2D and 3D and motions including rotations.

1.3. Contributions & Outline

This paper presents a TO methodology to design high-performance lightweight structures while also guaranteeing *accessibility* of every point on the design’s negative space for a given *collection* of cutting tool assemblies and fixtures (arbitrary shapes in 3D) and available motions including translations and rotations. The rotations can represent either a limited set of fixturing orientations for 3-axis milling, or a discrete sample of orientations that a 5-axis CNC system can reach.

Our approach does not impose any artificial limitations on geometric complexity of part, tools, and fixtures. It enables efficient and effective design space exploration to discover nontrivial geometries and topologies that are optimized for the specific machining capabilities of a machine shop. The constrained optimization is with regards to not only performance criteria (e.g., stiffness or strength) but also manufacturability, as opposed to the conventional approach that disregards the latter and postpones manufacturability concerns to downstream post-processing.

More specifically, the contributions of this paper are:

1. introducing a rigorous mathematical formulation of a continuous ‘inaccessibility measure field’ (IMF) in 3D design domain to modify the sensitivity field for TO;
2. formulating a TO framework that incorporates accessibility constraints for multi-axis machining based on realistic cutting tool assemblies and fixtures and arbitrary motions including translations and rotations;
3. developing efficient and flexible implementation of the IMF that enables balancing numerical accuracy against available time budget for calling within the TO alongside the finite element analysis (FEA);
4. implementing IMF on multi-core CPU/GPU for massive parallelization;
5. applying the accessibility constraints for multi-axis machining to density-based TO; and
6. demonstrating the effectiveness of our method by solving multiple benchmark and realistic examples in 2D and 3D on 2-, 3-, and 5-axis CNC machines.

2. Proposed Method

In this section, we will first discuss our analytic approach to accessibility analysis and introduce a continuous field to measure inaccessibility of a part with respect to a collection of tools and fixtures at a discrete set of fixturing orientations (Section 2.1). Next, we extend the TO formulation for incorporating multi-axis machining constraint into the density-based TO framework (Section 2.2).

2.1. Quantifying Multi-Axis Inaccessibility

TO typically starts with an initial design $\Omega := \Omega_0 \subset \mathbb{R}^3$ (called the *design domain*) and incrementally updates the design $\Omega \subseteq \Omega_0$ such that it remains within the design domain while minimizing the specified objective function and satisfying the specified constraints. These constraints may include performance criteria (e.g., stiffness or strength), evaluated by a physics solver such as FEA, as well as kinematic constraints (e.g., machine tool accessibility), which require spatial analysis. While the former is represented by (in)equality constraints in terms of real-valued functions, the latter is most naturally expressed using a set-theoretic language in terms of containment, interference, affine transformations, and Boolean operations. Here, we will present an analytic approach to convert the latter to (in)equality form to be used alongside the former.

On a multi-axis CNC machine, one deals with 6D rigid motions $(R, \mathbf{t}) \in \text{SE}(3)$, which are conceptualized as points in the *configuration space* (C-space) $\text{SE}(3)$, i.e., a pair formed by an special orthogonal (SO) automorphism of \mathbb{R}^3 (i.e., a 3D rotation) $R \in \text{SO}(3)$ and a vector (i.e., a 3D translation) $\mathbf{t} \in \mathbb{R}^3$. For 2- or 3-axis milling, the rotation component is fixed at a finite set of fixturing orientations, while the tool is swept along a continuum set of 2D or 3D translations. For 5-axis milling, there are two additional DOF for rotations, since the rotation around the tool axis is redundant.¹ The discrete fixturing orientations or continuum rotation DOF can be parameterized in a number of different ways, e.g., 3×3 orthogonal matrices, axis-angle pairs, unit quaternions, and Euler angles, or can be combined with the translational element to form unified representations such as 4×4 homogeneous matrices, dual quaternions, screws, etc. Each have their own pros and cons, which are well-understood. Our formulation is not restricted to a specific parameterization of $\text{SO}(3)$.

In practice, the workspace of the CNC machine is a bounded subset of $\text{SE}(3)$ which is digitized into a discrete set (i.e., finite sample) in accordance with the machine’s precision and required algorithmic accuracy.

For spatial planning, the obstacles $O := (\Omega \cup F)$ consist of the part/workpiece $\Omega \subset \mathbb{R}^3$ (i.e., evolving portion via TO) and the fixtures $F \subset \mathbb{R}^3$ (i.e., fixed portion), both of which are 3D pointsets represented in the same global coordinate frame. The tool assembly $T = (H \cup K)$ consists of the tool holder $H \subset \mathbb{R}^3$ (i.e., inactive portion) and the cutter $K \subset \mathbb{R}^3$ (i.e., active portion) represented in the same local coordinate frame, which is transformed by the *relative* rigid transformation $(R, \mathbf{t}) \in \text{SE}(3)$ with respect to the global coordinate frame of stationary obstacles.²

Assuming that the raw stock is the same as the design domain Ω_0 , the accessibility constraint can be formulated

¹The rapidly turning tool profile is typically modeled by its axisymmetric closure around the spindle axis (e.g., a flat/ball-end cylinder) rather than explicitly accounting for the rotation in C-space.

²In reality, both workpiece and tool assembly may move. Since accessibility depends only on relative motion, we can assume the former to be stationary without loss of generality.

as follows: for every point on the part’s exterior within the raw stock (i.e., the *negative space*) $(\Omega_0 - \Omega)$, there must exist a transformation $(R, \mathbf{t}) \in \text{SE}(3)$ that brings at least one point on the cutter (hereon called a *sharp point*) $\mathbf{k} \in K$ in contact with the query point, *without incurring a volumetric collision* between the objects in relative motion:

$$\begin{aligned} \forall \mathbf{x} \in (\Omega_0 - \Omega) : \quad & \exists (R, \mathbf{t}) \in \text{SE}(3) \text{ and } \exists \mathbf{k} \in K \\ \text{s.t. } \mathbf{x} = (R, \mathbf{t})\mathbf{k} = R\mathbf{k} + \mathbf{t} \text{ and } & O \cap^* (R, \mathbf{t})T = \emptyset, \end{aligned} \quad (1)$$

where the asterisk in \cap^* stands for regularization after intersection [47], i.e., touching only at the boundaries does not count as a collision, thus would not violate the above condition. $(R, \mathbf{t})T = RT + \mathbf{t}$ stands for the transformed tool assembly (rotation before translation).

2.1.1. Morphological Definition of Accessibility

The accessibility is commonly formulated in terms of the configuration space obstacle (C–obstacle) of relative transformations. The C–obstacle is defined as the set of all transformations that result in a collision, violating (1):

$$\mathcal{O} := \{(R, \mathbf{t}) \in \text{SE}(3) \mid O \cap^* (R, \mathbf{t})T \neq \emptyset\}. \quad (2)$$

The accessible region $A \subseteq \Omega_0$, defined by the set of all points in the design domain that satisfy (1), can be computed by *sweeping* (i.e., morphological dilation) of the cutter along the maximal collision-free motion. The latter is obtained as the complement of C–obstacle in the C–space (i.e., the ‘free space’) $\mathcal{O}^c = \text{SE}(3) - \mathcal{O}$, hence:

$$A(O, T, K) := \Omega_0 \cap \text{sweep}(\mathcal{O}^c, K) \quad (3)$$

$$= \Omega_0 \cap \bigcup_{(R, \mathbf{t}) \in \mathcal{O}^c} (RK + \mathbf{t}). \quad (4)$$

Both sweeps and C–obstacles can be expressed in terms of Minkowski products in C–space, and, in turn, as unions of the more familiar Minkowski sums in \mathbb{R}^3 if the rotations are factored out as follows [43]:

$$A(O, T, K) = \Omega_0 \cap \bigcup_{R \in \text{SO}(3)} (O \oplus (-RT))^c \oplus (RK), \quad (5)$$

in which $\oplus, \ominus, (\cdot)^c$ are the Minkowski sum, Minkowski difference, and set complement, respectively. For a given orientation $R \in \text{SO}(3)$, the first sum $D := O \oplus (-RT)$ is a translational ‘slice’ of the C–obstacle, whose complement D^c is the collection of all collision-free translations (i.e., a slice of \mathcal{O}^c for a fixed rotation). The second sum $D^c \oplus (RK)$ represents the accessible region for the same orientation, obtained by sweeping the rotated cutter RK along the maximal collision-free translation D^c . The inaccessible region $B \subseteq \Omega_0$ is the set of points in the raw stock that do not belong in A :

$$B(O, T, K) := \Omega_0 - A(O, T, K). \quad (6)$$

To convert the global set-theoretic definition of accessibility to a local (in)equality constraint, we use the correspondence between Minkowski and convolution algebras

for explicit and implicit morphology, respectively [43]. The indicator function of any pointset $X \subseteq \mathbb{R}^3$ is a binary-valued field denoted by $\mathbf{1}_X : \mathbb{R}^3 \rightarrow \{0, 1\}$ defined as:

$$\mathbf{1}_X(\mathbf{x}) = \begin{cases} 1 & \text{if } \mathbf{x} \in X; \\ 0 & \text{otherwise.} \end{cases} \quad \text{for any } X \subseteq \mathbb{R}^3. \quad (7)$$

Under fairly general regularity conditions,³ we have:

$$\mathbf{1}_D(\mathbf{t}) = \text{sign} \circ (\mathbf{1}_O * \tilde{\mathbf{1}}_{RT})(\mathbf{t}), \quad (8)$$

$$\mathbf{1}_A(\mathbf{x}) = \text{sign} \circ (-\mathbf{1}_D * \mathbf{1}_{RK})(\mathbf{x}), \quad (9)$$

where $*$ stands for the convolution operator defined for integrable fields over \mathbb{R}^3 , and $\mathbf{1}_{D^c}(\mathbf{t}) = -\mathbf{1}_D(\mathbf{t})$ where \neg stands for logical negation. We introduce the notation $\tilde{\mathbf{1}}_X(\mathbf{x}) = \mathbf{1}_{-X}(\mathbf{x}) = \mathbf{1}_X(-\mathbf{x})$ for reflection with respect to the origin, which is needed to match how convolutions are defined to attain their useful properties. The sign function is defined as $\text{sign}(x) = x/|x|$ if $x \neq 0$ and zero otherwise, and is required for algebraic closure—to convert the real-valued convolution to a binary-valued indicator function before passing it to the next convolution. See Appendix A for an explanation of the above identities. Fig. 2 illustrates both explicit and implicit operations in 2D.

While the indicator functions are useful for accessibility analysis as a post-TO test, we need a spatial field to penalize *inaccessibility* of different points within the candidate design $\Omega \subseteq \Omega_0$ to prevent the TO from violating accessibility at every iteration.

2.1.2. Inaccessibility Measure as Convolution

The no-collision condition in (1) can also be expressed in terms of the *measure* of intersection:

$$O \cap^* (R, \mathbf{t})T = \emptyset \iff \text{vol}[O \cap (R, \mathbf{t})T] = 0, \quad (10)$$

where $\text{vol}[\cdot]$ stands for volume (i.e., Lebesgue 3–measure) of a 3D pointset. This measure can be computed as an inner product of indicator functions, i.e., integration of their product over \mathbb{R}^3 . For objects in relative motion, the translational component results in a shift of function argument, turning the inner product into a convolution:

$$\text{vol}[O \cap (R, \mathbf{t})T] = \langle \mathbf{1}_O, \mathbf{1}_{(R, \mathbf{t})T} \rangle = (\mathbf{1}_O * \tilde{\mathbf{1}}_{RT})(\mathbf{t}), \quad (11)$$

which also appeared on the right-hand side of (8).

At a first glance, the convolution field appears like an ideal candidate for penalization in TO: a continuous field over \mathbb{R}^3 that measures inaccessibility. At a closer look, however, the domain of this function is the translational C–space, which is a different ‘type’ than the design domain. The former is a space of 3D displacement *vectors* (i.e., position *differences*) while the latter is of 3D *points*

³The correspondence is only valid if the participating sets are homogeneously 3D, e.g., the free space has no singularities, which is sufficient for our purposes. See [48] (Section 3.4) for details.

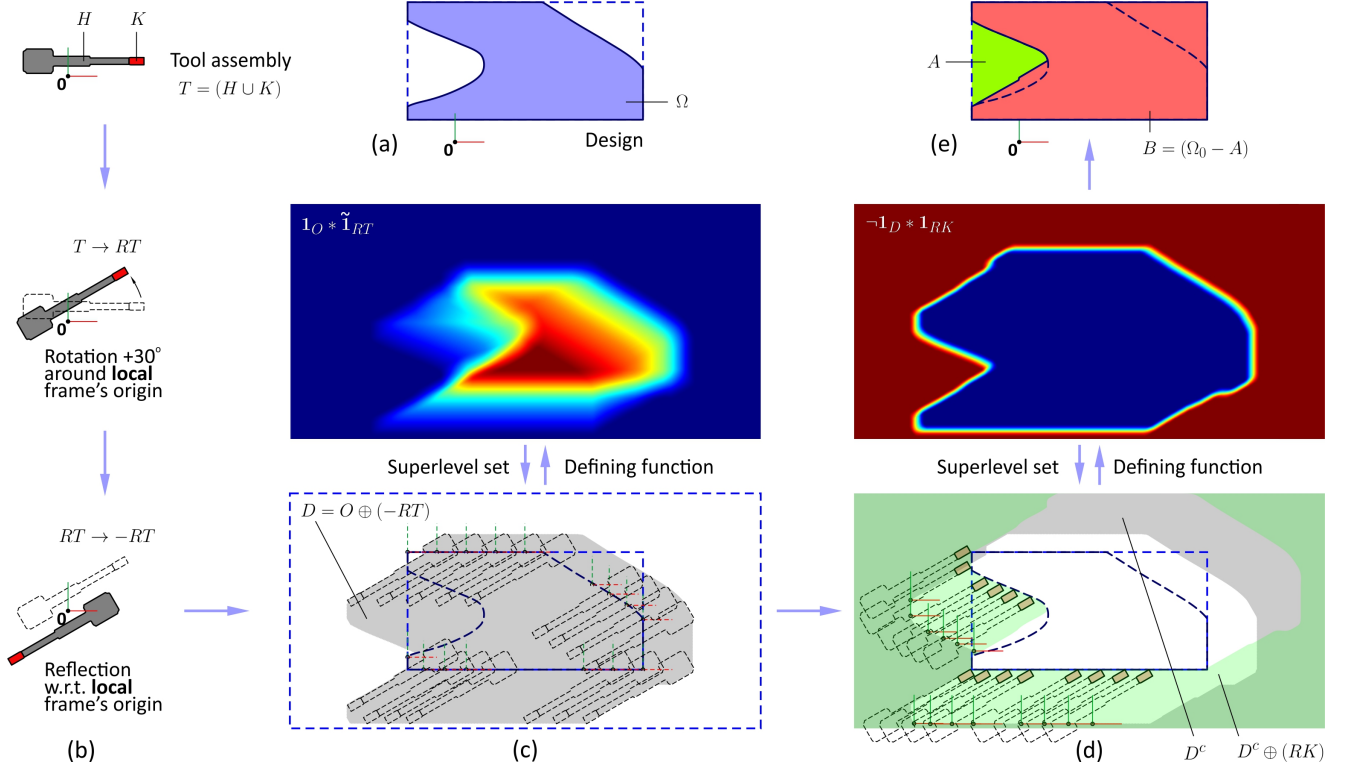


Figure 2: Consider (a) a 2D part $O = \Omega$ (here $F = \emptyset$) and (b) a 2D tool assembly $T = (H \cup K)$. The tool is re-oriented as $T \rightarrow RT$ for a given $R \in \text{SO}(2)$ and reflected as $RT \rightarrow -RT$. (c) The Minkowski sum $D = O \oplus (-RT)$ gives the set of colliding translations for the fixed rotation, which can be obtained as 0–superlevel set of a convolution $(\mathbf{1}_D * \tilde{\mathbf{1}}_{RT})$. (d) The Minkowski sum $D^c \oplus (RK)$ gives the accessible region as the sweep of the cutter along collision-free translations, which can be obtained as 0–superlevel set of a convolution $(-\mathbf{1}_D * \mathbf{1}_{RK})$. The decomposition into accessible A and inaccessible B regions is shown in (e).

(i.e., positions). The convolution function measures the inaccessibility for a hypothetical displacement of $\mathbf{t} \in \mathbb{R}^3$ that has nothing to do with any point $\mathbf{x} \in \Omega_0$. The function shifts with different choices of origin for the local coordinate system in which the tool assembly is described.

To properly “register” the shifted field with the design domain, we must select the origin at the sharp points so that the convolution $(\mathbf{1}_O * \tilde{\mathbf{1}}_{RT})(\mathbf{t})$ evaluated at the translation $\mathbf{t} \in \mathbb{R}^3$ returns the collision measure for shifting the sharp point from the origin $\mathbf{0}$ to $\mathbf{x} = (R, \mathbf{t})\mathbf{0} = R\mathbf{0} + \mathbf{t} = \mathbf{t}$. Since we have more than one option for the sharp point, each one provides an independent candidate for the origin to register the two spaces by shifting the convolution.

2.1.3. Inaccessibility for A Single Tool Assembly

We define the *inaccessibility measure field* (IMF) over the 3D design domain $f_{\text{IMF}} : \mathbb{R}^3 \rightarrow \mathbb{R}$ for each given tool assembly $T = (H \cup K)$ as the pointwise *minimum* of shifted convolutions for different choices of sharp points and available orientations $\Theta \subseteq \text{SO}(3)$ (which depends on T):

$$f_{\text{IMF}}(\mathbf{x}; O, T, K) := \min_{R \in \Theta} \min_{\mathbf{k} \in K} \text{vol}[O \cap (R, \mathbf{x})(T - \mathbf{k})]. \quad (12)$$

There are two independent transformations in effect:

- The shift $T \rightarrow (T - \mathbf{k})$ in (12) is to try different ways to register the translation space with the design domain,

by changing the local coordinate system to bring different sharp points to the origin.

- The rotation $(T - \mathbf{k}) \rightarrow (RT - R\mathbf{k})$ followed by translation $(RT - R\mathbf{k}) \rightarrow (RT - R\mathbf{k}) + \mathbf{x}$ bring the candidate sharp point (new origin) to the query point $\mathbf{x} \in \Omega_0$.

The same effect can be obtained by querying the convolution in (11) at $\mathbf{t} := (\mathbf{x} - R\mathbf{k})$ so that the rigid transformation (R, \mathbf{t}) brings the sharp point in contact with the query point: $(R, \mathbf{t})\mathbf{k} = R\mathbf{k} + \mathbf{t} = R\mathbf{k} + (\mathbf{x} - R\mathbf{k}) = \mathbf{x}$, as expected. The IMF is thus computed as follows:

$$f_{\text{IMF}}(\mathbf{x}; O, T, K) = \min_{R \in \Theta} \min_{\mathbf{k} \in K} (\mathbf{1}_O * \tilde{\mathbf{1}}_{RT})(\mathbf{x} - R\mathbf{k}). \quad (13)$$

Each transformed convolution measures the collision for an attempt to remove the query point $\mathbf{x} \in \Omega_0$ in the candidate orientation $R \in \Theta$ with the sharp point $\mathbf{k} \in K$. The inaccessibility of the query point is determined by the orientation and sharp point that result in the *best case* scenario, i.e., the least collision volume.

Figure 3 illustrates the idea behind (13) for simple 2D shapes with a few candidate orientations and sharp points. Note that the collision measure accounts for both: 1) penetrations of the cutter into the local neighborhood of the part (often referred to as “gouging” [38]) or fixtures, which leads to over-cutting; and 2) global interferences that may occur elsewhere along the tool holder.

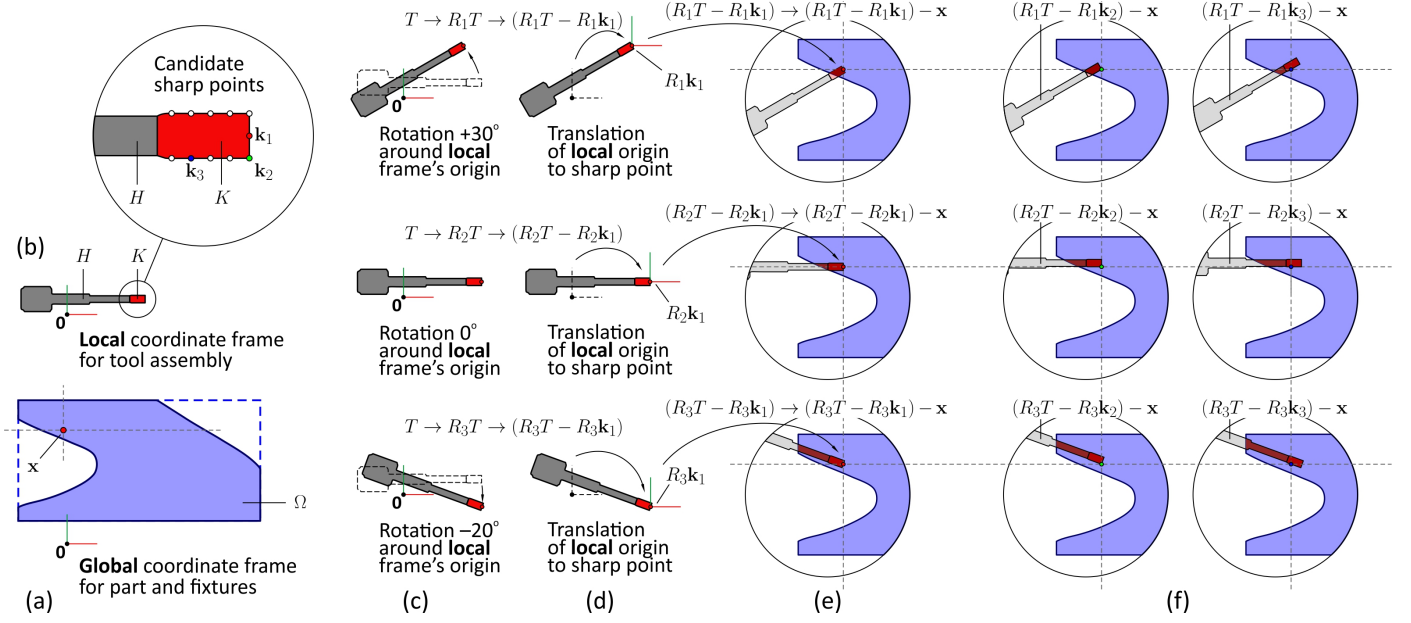


Figure 3: Consider (a) a 2D part and (b) a 2D tool assembly. At a given query point $\mathbf{x} \in \Omega_0$, the IMF is computed by looking at different rotations $R_1, R_2, R_3, \dots \in \Theta$ of the tool assembly, 3 of which are shown in (c). For each oriented tool $T \rightarrow R_i T$, the origin is shifted to different sharp points $\mathbf{k}_1, \mathbf{k}_2, \mathbf{k}_3, \dots \in K$; e.g., for the (rotated) sharp point $R_i \mathbf{k}_j \in R_i K$, the tool is translated as $R_i T \rightarrow (R_i T - R_i \mathbf{k}_j)$ shown in (d). The new origin is brought in contact with the query point, hence $(R_i T - R_i \mathbf{k}_j) \rightarrow (R_i T - R_i \mathbf{k}_j) - \mathbf{x}$ shown in (e). This is repeated for all candidate sharp points (f) and the IMF is computed as the minimum over all rotations and sharp points.

The IMF can be used to classify the design domain into disjoint subsets $A := f_{\text{IMF}}^{-1}(0)$, and $B = \Omega_0 - A$:

$$A(O, T, K) := \{\mathbf{x} \in \Omega_0 \mid f_{\text{IMF}}(\mathbf{x}; O, T, K) = 0\},$$

$$B(O, T, K) := \{\mathbf{x} \in \Omega_0 \mid f_{\text{IMF}}(\mathbf{x}; O, T, K) > 0\}.$$

which are the same as the pointsets defined in (4) and (6) if $\Theta := \text{SO}(3)$, under quite general conditions. A query point is accessible iff its IMF is zero, i.e., there exists one or more tool orientations and sharp points with which the query point can be touched without incurring a collision.

Note that every point inside the design itself is inaccessible, i.e., $\Omega \subseteq B$ thus $(\Omega \cap A) = \emptyset$. Hence, the inaccessible region can be further decomposed into two disjoint subsets, the part Ω and $\Gamma := (B - \Omega)$, to which we refer as the ‘secluded region’. The latter is the set of all points in the negative space $(\Omega_0 - \Omega)$ of the part/workpiece that are inaccessible, i.e., points in the raw stock that cannot be machined at any orientation with the given tool using the specified options for sharp points. Figure 4 illustrates this three-way decomposition for a 2D example.

For parts designed for machining, TO must resist generating secluded regions, including nucleation of internal voids inside the part, which are often seen in TO parts meant for AM.

2.1.4. Inaccessibility for Multiple Tool Assemblies

Given $n_T \geq 1$ available tool assemblies $T_i = (H_i \cup K_i)$ for $1 \leq i \leq n_T$, we compute their combined IMF by applying another minimum operation over different tools to

identify the tool(s) with the smallest volumetric interference at available orientations and sharp points:

$$f_{\text{IMF}}(\mathbf{x}; O) := \min_{1 \leq i \leq n_T} f_{\text{IMF}}(\mathbf{x}; O, T_i, K_i) \quad (14)$$

in which $f_{\text{IMF}}(\mathbf{x}; O, T_i, K_i)$ are computed from (13). Once again, we can decompose the design domain into accessible and inaccessible regions, respectively, with respect to all available tool assemblies:

$$A(O) := \bigcup_{1 \leq i \leq n_T} A(O, T_i, K_i), \quad (15)$$

$$B(O) := \bigcap_{1 \leq i \leq n_T} B(O, T_i, K_i). \quad (16)$$

in which $A(O, T_i, K_i)$ and $B(O, T_i, K_i)$ were obtained earlier. The secluded region with respect to all tools is the subset of inaccessible regions that lies outside the design:

$$\Gamma(O) := B(O) \cap (\Omega_0 - \Omega) = B(O) - \Omega. \quad (17)$$

2.1.5. Algorithm to Support Density-Based TO

In density-based TO, one deals with a continuous density function $\rho_\Omega : \Omega \rightarrow [0, 1]$ to represent intermediate designs, rather than indicator functions. While we can use a threshold $0 < \tau < 1$ (e.g., $\tau := 0.5$) to define the indicator functions as $\mathbf{1}_\Omega(\mathbf{x}) := 1$ iff $\rho_\Omega(\mathbf{x}) > \tau$ for use in (13), our experience shows that direct use of the density function works better to provide additional smoothing:

$$f_{\text{IMF}}(\mathbf{x}; \rho_O, T, K) := \min_{R \in \Theta} \min_{\mathbf{k} \in K} (\rho_O * \tilde{\mathbf{1}}_{RT})(\mathbf{x} - R\mathbf{k}). \quad (18)$$

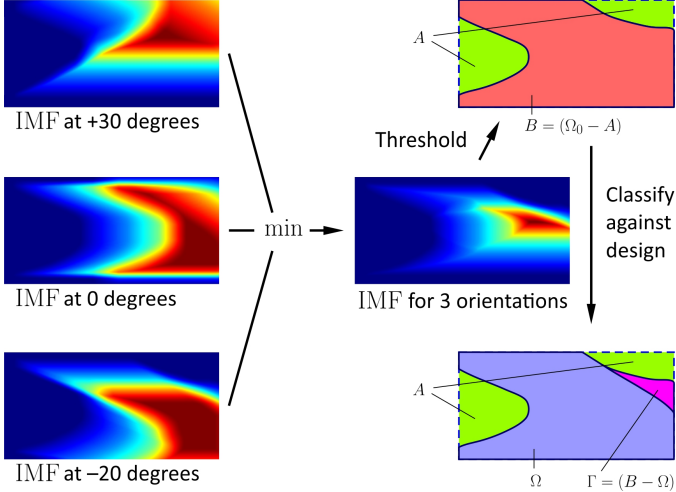


Figure 4: For every candidate orientation in Fig. 3 (c), the minimum of convolution over all sharp points is computed. The overall IMF is obtained as another minimum over all orientations, whose zero/nonzero values determine accessible/inaccessible regions.

The function $\rho_O : \Omega_0 \rightarrow [0, 1]$ can be obtained as: $\rho_O(\mathbf{x}) := \rho_\Omega(\mathbf{x}) + \mathbf{1}_F(\mathbf{x})$, in which $\rho_\Omega(\mathbf{x})$ is obtained directly from TO. The combined IMF for all tool assemblies $f_{\text{IMF}}(\mathbf{x}; \rho_O)$ is computed as:

$$f_{\text{IMF}}(\mathbf{x}; \rho_O) := \min_{1 \leq i \leq n_T} f_{\text{IMF}}(\mathbf{x}; \rho_O, T_i, K_i) \quad (19)$$

The IMF is in units of volume. To use it alongside other constraints in TO (e.g., stiffness and strength) we first normalize it by the global maximum to obtain $\bar{f}_{\text{IMF}}(\mathbf{x}; \rho_O)$.

Moreover, to deal with inaccuracies due to discretization and intermediate densities in TO, we allow for some relaxation, aiming for a small allowance of $0 < \lambda \ll 1$ (e.g., $\lambda := 0.01$) for nonzero inaccessibility. In other words, we only penalize the points that have (normalized) inaccessibility value of greater than the threshold λ .

For the sake of generality, we assume that a given tool assembly T_i comes with a given set of rotations $\Theta_i \subset \text{SO}(3)$ available for orienting that tool. For 3-axis milling, the set of available rotations is finite, corresponding to different fixturing configurations. For 5-axis milling, we can assume a continuum set of rotations, which can be sampled for computational purposes.

In practice, the shape of fixtures F hence $O = (\Omega \cup F)$ can change every time the part is rotated and re-clamped for 3-axis milling at a different orientation. For clarity, we do not consider multiple fixtures in this paper, although accounting for their changing shapes comes at no extra cost as long as the fixturing setup is given a priori.

Algorithm 1 describes the subroutine that computes the IMF for a given candidate design and a specified set of tool assemblies, orientations, and fixtures for use within TO iterations. For every tool assembly represented by a 3D array $[\mathbf{1}_{T_i}]$ of binary values (i.e., voxels) and a given orientation $R \in \Theta_i$ represented by a unit quaternion, the 3D array $[\tilde{\mathbf{1}}_{RT_i}]$ is obtained by rotation and re-sampling

on the uniform grid, followed by a reflection with respect to the origin.⁴ The discretized convolution is represented as a 3D array $[\rho_O * \tilde{\mathbf{1}}_{RT_i}]$ and is computed by two forward FFTs on $[\rho_O]$ and $[\tilde{\mathbf{1}}_{RT_i}]$, a pointwise multiplication in the frequency domain, and an inverse FFT back to the physical domain (of translations). This is repeated for all tools and orientations to obtain the minimums in (18). See Appendix B for an analysis of time and space complexity.

Algorithm 1 Compute $[\bar{f}_{\text{IMF}}], [\mathbf{1}_{\Gamma(O)}]$.

```

procedure IMF( $[\rho_\Omega], [\mathbf{1}_F], [\mathbf{1}_{H_i}], [\mathbf{1}_{K_i}], \{\Theta_i\}; \lambda, n_T$ )
  Define  $[\rho_O] \leftarrow [\rho_\Omega] + [\mathbf{1}_F]$   $\triangleright$  Implicit union
  Initialize  $[f_{\text{IMF}}] \leftarrow 0$   $\triangleright$  IMF for all the tools
  for  $i \leftarrow 1$  to  $n_T$  do
    Define  $[\mathbf{1}_{T_i}] \leftarrow [\mathbf{1}_{H_i}] + [\mathbf{1}_{K_i}]$   $\triangleright$  Implicit union
    Initialize  $[\gamma_i] \leftarrow [0]$   $\triangleright$  IMF for the  $i^{\text{th}}$  tool
    for all  $R \in \Theta_i$  do
       $[\mathbf{1}_{RT_i}] \leftarrow \text{ROTATE}([\mathbf{1}_{T_i}], R)$   $\triangleright$  Re-sampling
       $[\tilde{\mathbf{1}}_{RT_i}] \leftarrow \text{REFLECT}([\mathbf{1}_{RT_i}])$ 
       $[g_i] \leftarrow \text{CONVOLVE}([\rho_O], [\tilde{\mathbf{1}}_{RT_i}])$   $\triangleright$  FFT-based
      for all  $\mathbf{k} \in \text{SUPPORT}([\mathbf{1}_{K_i}])$  do
         $[h_i] \leftarrow \text{TRANSLATE}([g_i], -R\mathbf{k})$ 
         $[\gamma_i] \leftarrow \min([\gamma_i], [h_i])$   $\triangleright$  Over sharp points
      end for
    end for
     $[f_{\text{IMF}}] \leftarrow \min([f_{\text{IMF}}], [\gamma_i])$   $\triangleright$  Over all tools
  end for
   $[\bar{f}_{\text{IMF}}] \leftarrow [f_{\text{IMF}}] / \text{MAX}([f_{\text{IMF}}])$   $\triangleright$  Normalization
   $[\mathbf{1}_{B(O)}] \leftarrow [f_{\text{IMF}} > \lambda]$ 
   $[f_{\text{IMF}}] \leftarrow [f_{\text{IMF}}] \cdot [\mathbf{1}_{B(O)}]$   $\triangleright$  Add allowance
   $[\mathbf{1}_{\Gamma(O)}] \leftarrow [\mathbf{1}_{\Omega_0}] \cdot [\neg \mathbf{1}_\Omega] \cdot [\mathbf{1}_{B(O)}]$   $\triangleright$  Implicit intersect
  return  $([\bar{f}_{\text{IMF}}], [\mathbf{1}_{\Gamma(O)}])$ 
end procedure

```

Our formulation in terms of sharp points allows immense flexibility for balancing accuracy against computation time. As the cutter’s boundary is sampled more densely, the IMF can only decrease in value due to the minimum operation in (13), and the set of secluded points $\Gamma(O)$ grows in size. This comes at a small cost of more queries on the convolution. Importantly, coarser sampling of the cutter can only *over-estimate* the exact IMF, leading to a *conservative* approximation of inaccessibility. As more sharp points are sampled on the cutter, more candidate designs are deemed machinable by carving out their negative spaces via the same sample points. Omitting other sharp points can over-constrain the TO by “false positives” in collision detection, i.e., obtaining $f_{\text{IMF}}(\mathbf{x}; \Omega) > 0$ while the true value is zero; however, the approximation never violates the exact form of accessibility constraint.

It is worthwhile noting that our model of inaccessibility does not distinguish between different modes of collision

⁴The reflection is conveniently implemented as a conjugation in the frequency domain after FFT (Hermitian symmetry).

such as local over-cutting (i.e., gouging) and global interferences with part/fixtures. Our initial TO experiments showed that defining different collision measures and using unequal weights when penalizing them in TO show no notable improvement in the TO results. In fact, imbalanced weighting can result in tolerating one type of collision in favor of another, resulting in undesirable design artifacts.

2.2. Machining-Constrained Topology Optimization

Based on the accessibility analysis discussed in Section 2.1, we formulate the TO problem as:

$$\text{Minimize}_{\Omega \subseteq \Omega_0} \varphi(\Omega), \quad (20a)$$

$$\text{such that } [\mathbf{K}_\Omega][\mathbf{u}_\Omega] = [\mathbf{f}], \quad (20b)$$

$$V_\Omega \leq V_{\text{target}}, \quad (20c)$$

$$V_{\Gamma(O)} = 0, \quad (20d)$$

where $\varphi(\Omega) \in \mathbb{R}$ is the value of objective function for a given design $\Omega \subseteq \Omega_0$. $[\mathbf{f}]$, $[\mathbf{u}_\Omega]$, and $[\mathbf{K}_\Omega]$ are (discretized) external force vector, displacement vector, and stiffness matrix, respectively, for FEA. $V_\Omega := \text{vol}[\Omega]$ represents the design volume and $V_{\text{target}} > 0$ is the volume budget. The accessibility constraint for machining is imposed via (20d) by asserting that the secluded $V_{\Gamma(O)} := \text{vol}[\Gamma(O)]$ (i.e., volume of inaccessible regions in the negative space) must be zero. In practice, we impose a small nonzero upper-bound $\sim 1\%$ of part's volume) to provide relaxation against discretization errors. This initial formulation of accessibility as a 'global' constraint makes it difficult to incorporate into TO, as computing a local gradient/sensitivity for the inaccessible volume with respect to design variables is theoretically challenging, due to inherent discontinuities in collision detection, and computationally prohibitive. However, we showed in [45] that by formulating the inaccessibility as a 'local' constraint $\bar{f}_{\text{IMF}}(\mathbf{x}) \leq \lambda$ for all $\mathbf{x} \in (\Omega_0 - \Omega)$, the continuous IMF can be directly augmented into the sensitivity field to filter out the inaccessible regions of the design domain.

Putting aside the accessibility constraint in (20d) for the moment, the more familiar constrained optimization problem of (20a) through (20c) can be expressed as minimization of the following Lagrangian:

$$\mathcal{L}_\Omega := \varphi(\Omega) + \lambda_1 \left(\frac{V_\Omega}{V_{\text{target}}} - 1 \right) + [\lambda_2]^T \left([\mathbf{K}_\Omega][\mathbf{u}_\Omega] - [\mathbf{f}] \right). \quad (21)$$

Using the prime symbol $(\cdot)'$ to represent the generic (i.e., representation-agnostic) differentiation of a function with respect to Ω , we obtain (via chain rule):

$$\mathcal{L}'_\Omega = \varphi'(\Omega) + \lambda_1 \frac{V'_\Omega}{V_{\text{target}}} + [\lambda_2]^T \left([\mathbf{K}_\Omega][\mathbf{u}_\Omega] \right)', \quad (22)$$

$$\begin{aligned} &= \left(\left[\frac{\partial \varphi}{\partial \mathbf{u}} \right] + [\lambda_2]^T [\mathbf{K}_\Omega] \right) [\mathbf{u}'_\Omega] \\ &+ \lambda_1 \frac{V'_\Omega}{V_{\text{target}}} + [\lambda_2]^T [\mathbf{K}'_\Omega][\mathbf{u}_\Omega]. \end{aligned} \quad (23)$$

Since computing $[\mathbf{u}'_\Omega]$ requires solving (20d) as many times as the number of design variables and is computationally prohibitive, $[\lambda_2]$ is chosen as the solution to the adjoint problem [1] which reduces (23) to:

$$\mathcal{L}'_\Omega = \lambda_1 \frac{V'_\Omega}{V_{\text{target}}} + [\lambda_2]^T [\mathbf{K}'_\Omega][\mathbf{u}_\Omega], \quad (24)$$

$$\text{if } [\lambda_2] := -[\mathbf{K}_\Omega]^{-1} \left[\frac{\partial \varphi}{\partial \mathbf{u}} \right].$$

When the objective function is the design's compliance under the applied load; namely, $\varphi(\Omega) := [\mathbf{f}]^T [\mathbf{u}_\Omega]$, we obtain $[\lambda_2] = -[\mathbf{u}_\Omega]$. This dramatically simplified the problem as the compliance is self-adjoint, i.e., there is no need for solving an additional adjoint problem unlike the case with other objective functions (e.g., stress).

To incorporate the accessibility constraint for multi-axis machining, we modify the sensitivity field \mathcal{S}_Ω as follows:

$$\mathcal{S}_\Omega := (1 - w_{\text{acc}}) \bar{\mathcal{S}}_\varphi + w_{\text{acc}} \bar{\mathcal{S}}_{\text{IMF}}, \quad (25)$$

where $0 \leq w_{\text{acc}} < 1$ is the filtering weight for accessibility, and can be either a constant or adaptively updated based on the secluded volume $V_{\Gamma(O)}$. $\bar{\mathcal{S}}_\varphi$ is the normalized sensitivity field with respect to the objective function, i.e., only the second term $[\lambda_2]^T [\mathbf{K}'_\Omega][\mathbf{u}_\Omega]$ on the right hand side of (24), noting that the volume constraint is satisfied with the optimality criteria iteration [49]. $\bar{\mathcal{S}}_{\text{IMF}}$ is the normalized accessibility filter defined in terms of the normalized IMF as:

$$\bar{\mathcal{S}}_{\text{IMF}}(\mathbf{x}) := \begin{cases} \bar{f}_{\text{IMF}}(\mathbf{x}; \rho_O) & \text{if } \mathbf{x} \in \Omega, \\ 1 & \text{if } \mathbf{x} \in \Gamma(O), \\ 0 & \text{otherwise.} \end{cases} \quad (26)$$

in which $O = (\Omega \cup F)$ and $\rho_O(\mathbf{x}) = \rho_\Omega(\mathbf{x}) + \mathbf{1}_F(\mathbf{x})$ represent the design and fixtures, explicitly and implicitly. $\bar{f}_{\text{IMF}}(\mathbf{x}; \rho_O)$ is obtained from (19) (after normalization by its maximum) and $\Gamma(O) = B(O) - \Omega = B(O) \cap \Omega^c$ represents the secluded regions, i.e., inaccessible portion of the negative space, define in (17). Since we are working with implicit representations, the first condition $\mathbf{x} \in \Omega$ in (26) is computed by $\mathbf{1}_\Omega(\mathbf{x}) = 1$, i.e., $\rho_\Omega(\mathbf{x}) > \tau$. The second condition $\mathbf{x} \in \Gamma(O)$ is computed as a conjunction of $\bar{f}_{\text{IMF}} > \lambda$ (for $\mathbf{x} \in B(O)$) and $\rho_\Omega(\mathbf{x}) \leq \tau$ (for $\mathbf{x} \in \Omega^c$).

The expressions in (20) through (26) are general and representation-agnostic, and can be used in both density-based and levelset TO. To generate the results of this paper, we use the method of solid isotropic material with penalization (SIMP). The implicit design representation $\rho_\Omega : \Omega_0 \rightarrow [0, 1]$ used in the definition of IMF is obtained as the projection of another field $\xi_\Omega : \Omega_0 \rightarrow [0, 1]$ (smoother density field for design exploration) whose discretization $[\xi_\Omega]$ is used as SIMP design variables. We use the following Heaviside projection [50]:

$$\rho_\Omega(\mathbf{x}) = 1 - e^{-\beta \xi_\Omega(\mathbf{x})} + \xi_\Omega(\mathbf{x}) e^{-\beta}, \quad (27)$$

We use $\beta := 2$ for 2D and $\beta := 8$ for 3D examples of Section 3. Algorithm 2 describes the accessibility-constrained TO

using SIMP. The sensitivity field is augmented using the IMF output of Algorithm 1.

Algorithm 2 TO with multi-axis machining constraint.

```

procedure TO( $[\mathbf{f}]$ ,  $V_{\text{target}}$ ,  $[\mathbf{1}_{H_i}]$ ,  $[\mathbf{1}_{K_i}]$ ,  $\{\Theta_i\}$ ;  $\lambda$ ,  $n_T$ ,  $\beta$ ,  $\delta$ ,  $l$ )
  Initialize  $[\xi_\Omega] \leftarrow [V_{\text{target}}/\text{INTEGRAL}([\mathbf{1}_{\Omega_0})]$ 
  Initialize  $\Delta \leftarrow \infty$ 
  Initialize  $iter \leftarrow 0$ 
  while  $\Delta > \delta$  and  $iter < l$  do
     $[\rho_\Omega] \leftarrow \text{HEAVISIDE}([\xi_\Omega], \beta)$   $\triangleright$  Projection
     $[\mathbf{u}] \leftarrow \text{FEA}([\rho_\Omega], [\mathbf{f}])$   $\triangleright$  Solve FEA
     $\varphi(\Omega) \leftarrow \text{EVALUATE}([\rho_\Omega], [\mathbf{u}])$   $\triangleright$  Obj. func.
     $[\mathcal{S}_\varphi] \leftarrow \text{GRADIENT}([\rho_\Omega], [\mathbf{u}], \varphi(\Omega))$   $\triangleright$  Sensitivity
     $[\rho_Q] \leftarrow [\rho_\Omega] + [\mathbf{1}_F]$   $\triangleright$  Implicit union
     $([\hat{f}_{\text{IMF}}], [\mathbf{1}_{\Gamma(O)}]) \leftarrow \text{IMF}([\rho_\Omega], [\mathbf{1}_F], \dots; \lambda, n_T)$ 
       $\triangleright$  Call Algorithm 1 with obvious arguments
     $[\mathcal{S}_{\text{IMF}}] \leftarrow \text{PENALIZE}([\hat{f}_{\text{IMF}}], [\mathbf{1}_{\Gamma(O)}])$   $\triangleright$  Eq. (26)
     $[\mathcal{S}] \leftarrow (1 - w_{\text{acc}})[\mathcal{S}_\varphi] + w_{\text{acc}}[\mathcal{S}_{\text{IMF}}]$   $\triangleright$  Eq. (25)
     $[\xi_\Omega^{\text{new}}] \leftarrow \text{UPDATE}([\xi_\Omega], [\mathcal{S}])$   $\triangleright$  SIMP filtering
     $\Delta \leftarrow \text{INTEGRATE}([\xi_\Omega^{\text{new}}] - [\xi_\Omega])$   $\triangleright$  Vol. diff.
     $iter \leftarrow iter + 1$   $\triangleright$  Iter. counter
     $[\xi_\Omega] \leftarrow [\xi_\Omega^{\text{new}}]$   $\triangleright$  For next iteration
  end while
  return  $[\xi_\Omega]$ 
end procedure

```

3. Results

In this section, we will present benchmark and realistic examples in 2D and 3D. All results are generated using a SIMP implementation, where the optimality criteria method was used to update the density field.

All examples are run on a desktop machine with Intel[®] Core[™] i7-7820X CPU with 8 processors running at 4.5 GHz, 32 GB of host memory, and an NVIDIA[®] GeForce[®] GTX 1080 GPU with 2,560 CUDA cores and 8 GB of device memory.

3.1. Benchmark Example: Cantilever Beam

First, we consider a simple cantilever beam example in 2D and 3D. The loading conditions are shown in Fig. 5. We use material properties of Stainless Steel with Young’s modulus of $E = 270$ GPa and Poisson ratio of $\nu = 0.3$. In each example, we solve both accessibility-constrained and unconstrained TO and report the nonzero secluded volume for the latter $V_{\Gamma_{\text{unc}}} > 0$ whose prevention comes at the cost of an increase in compliance results ($\varphi_{\text{con}} > \varphi_{\text{unc}}$).

In 2D, we set the volume fraction to 0.5 and optimize the design for minimal compliance with and without accessibility constraints for machining at resolution 256×128 . The accessibility constraint is defined using two cutting tool assemblies of nontrivial shapes, one with a thinner and another with a thicker cutting edge. Fig. 6 illustrates the accessibility-unconstrained optimized cantilever beam at

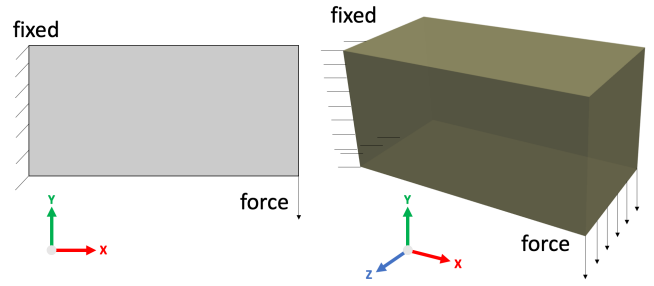


Figure 5: Cantilever beam boundary conditions in 2D and 3D.

0.5 volume fraction and accessibility analysis based on the cutting tool with thin cutter with $(+1, 0)$ tool direction.

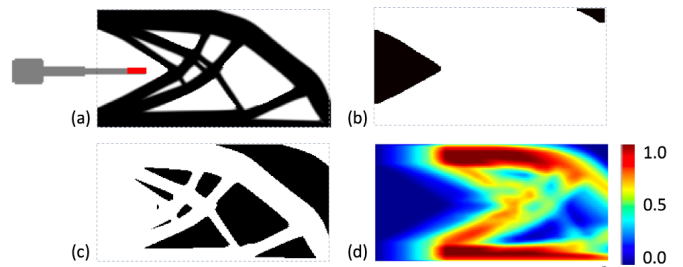


Figure 6: Accessibility-unconstrained TO for cantilever beam in 2D: (a) optimized cantilever beam at volume fraction of 0.5 and the oriented end-mill tool, (b) set of collision-free translations of cutter, (c) secluded regions, and (d) normalized IMF.

At first, let us consider only a few orientations per tool, one-at-a-time, for which the tool configuration and the optimized designs are depicted in Fig. 7 (b, c).

Observe that imposing accessibility constraints prevents nucleation of interior holes in the optimized design. Further, the shape of cutter can alter the accessible region at each iteration and IMF, subsequently changing the final design. Table 1 summarizes the results for compliance and secluded volume in 2D for the tool in Fig. 7 (a) for accessibility-unconstrained and constrained cases. Fig. 8 shows convergence of compliance for the 2D benchmark example with the thin cutter.

Fig. 9 illustrates the optimized cantilever beam in 3D at volume fraction of 0.3 with milling tools approaching from different directions in 3D. Table 2 summarizes the results for compliance and inaccessible volume for 3D cases.

Table 3 summarizes the benchmarking of computational efficiency for FEA and IMF computations. FEA is solved using conjugate gradients and sparse matrix-vector multiplications, while IMF is computed using convolutions via FFTs and vectorized minimization over 4D arrays. Both computations are performed on the GPU. According to clock times presented in Table 3, FEA is the computational bottleneck as FFTs are extensively optimized for GPU computing (using ArrayFire and cuFFT). However, since standard FFTs work with dense matrices as opposed to FEA that can exploit sparsity, IMF computation is the memory bottleneck on the GPU. Note that the design res-

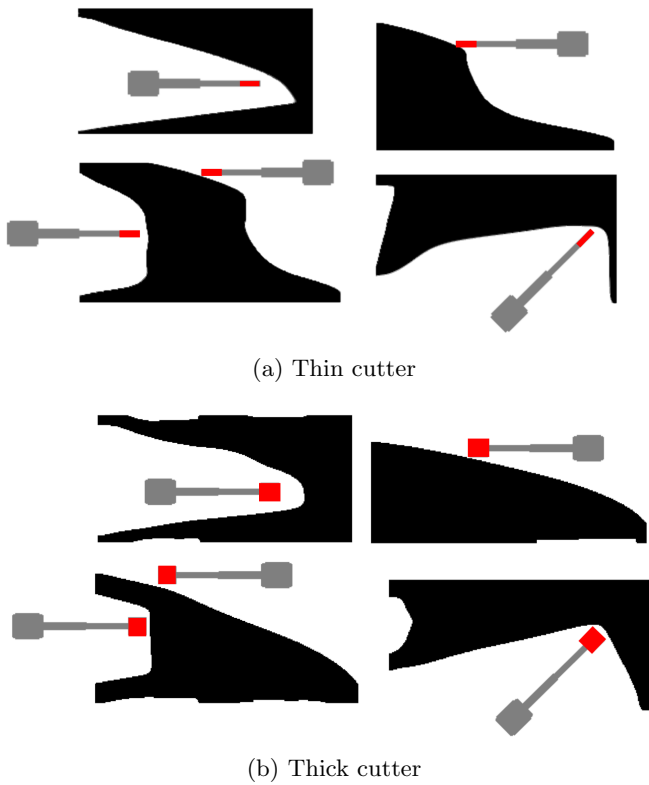


Figure 7: Benchmark cantilever beam example in 2D at a volume fraction of 0.5. The accessibility constraint is imposed at 8 different configurations with two endmill cutter profiles.

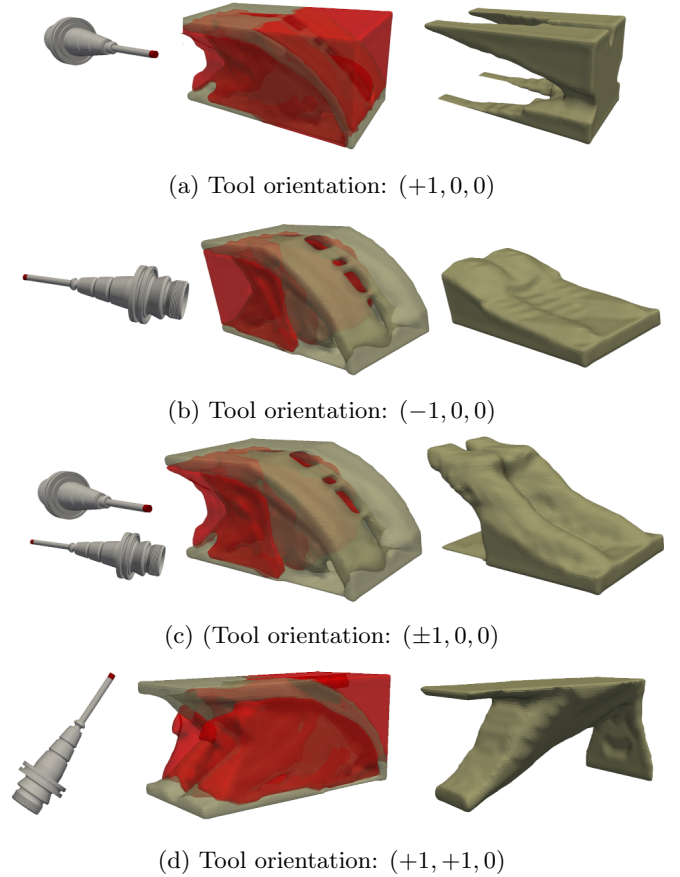


Figure 9: Benchmark cantilever beam example in 3D at 0.3 volume fraction, using different tool orientation combinations. Secluded regions are shown in red.

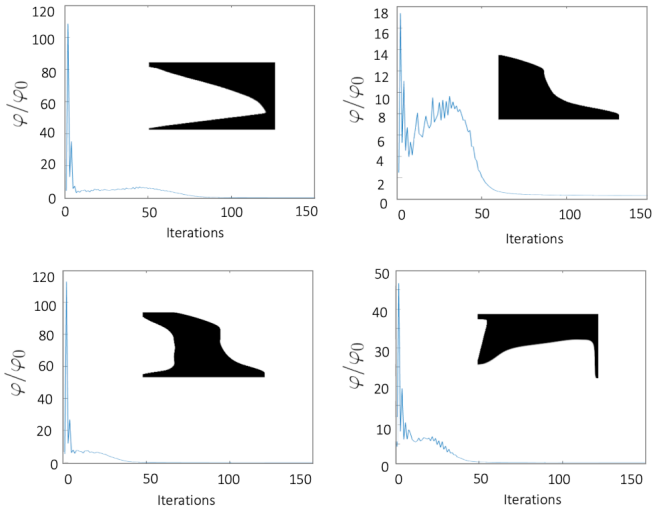


Figure 8: Convergence plots for 2D benchmark examples with thin cutter. φ and φ_0 are compliance and compliance of the initial design with uniform density of 0.5.

olution used in TO also dictates the tool and fixture resolutions to use the FFT-based convolution.

Table 1: Summary of cantilever beam results in 2D.

Tool direction	$\frac{V_{\Gamma_{\text{unc}}}}{V_{\Omega_0}}$	$\frac{\varphi_{\text{con}}}{\varphi_{\text{unc}}}$	w_{acc}	λ
(+1, 0)	0.32	4.2	0.5	0.05
(-1, 0)	0.32	2.4	0.5	0.05
(±1, 0)	0.16	1.3	0.5	0.05
(+1, +1)	0.40	3.7	0.5	0.05

Table 2: Summary of cantilever beam results in 3D.

Tool direction	$\frac{V_{\Gamma_{\text{unc}}}}{V_{\Omega_0}}$	$\frac{\varphi_{\text{con}}}{\varphi_{\text{unc}}}$	w_{acc}	λ
(+1, 0, 0)	0.48	8.57	0.5	0.025
(-1, 0, 0)	0.53	8.57	0.5	0.010
(±1, 0, 0)	0.37	2.86	0.5	0.010
(+1, +1, 0)	0.54	2.38	0.5	0.010

3.2. GE Bracket: 3-Axis Milling with Eye-Bolt Fixtures

Next, let us consider the example of GE bracket shown in Fig. 10. The material is Titanium with elastic proper-

Table 3: Computational time and memory of FEA vs. IMF computation using FFTs.

Part Resolution		Tool Resolution		Clock Time (sec)		Memory (MB)	
				FEA	IMF	FEA	IMF
$37 \times 37 \times 74$	$\approx 1.0 \times 10^5$	$142 \times 142 \times 142$	$\approx 2.9 \times 10^6$	2.14	0.26	190	1390
$47 \times 47 \times 93$	$\approx 2.3 \times 10^5$	$180 \times 180 \times 178$	$\approx 5.8 \times 10^6$	5.68	0.48	386	2820
$54 \times 54 \times 107$	$\approx 3.1 \times 10^5$	$207 \times 207 \times 205$	$\approx 8.8 \times 10^6$	9.97	0.48	586	4270
$59 \times 59 \times 117$	$\approx 4.1 \times 10^5$	$226 \times 226 \times 224$	$\approx 1.1 \times 10^7$	14.25	0.48	764	5580
$63 \times 63 \times 125$	$\approx 5.0 \times 10^5$	$241 \times 241 \times 241$	$\approx 1.4 \times 10^7$	16.03	0.48	938	6810

Table 4: Summary of GE multi-axis results.

Tool direction(s)	$\frac{V_{\Gamma_{\text{unc}}}}{V_{\Omega_0}}$	$\frac{\varphi_{\text{con}}}{\varphi_{\text{unc}}}$	w_{acc}	λ
(+1, 0, 0)	0.09	1.93	0.5	0.025
(0, ±1, 0)	0.11	2.73	0.5	0.025
(0, 0, +1)	0.14	1.66	0.5	0.025
(-1, 0, -1)	0.19	2.53	0.5	0.025
$\left\{ \begin{array}{l} (\pm 1, 0, 0) \\ (0, \pm 1, 0) \\ (0, 0, \pm 1) \end{array} \right.$	0.00	1.13	0.1	0.025

ties of $E = 113.8$ GPa and $\nu = 0.34$. The initial design domain is discretized into 100,000 hexahedral elements.

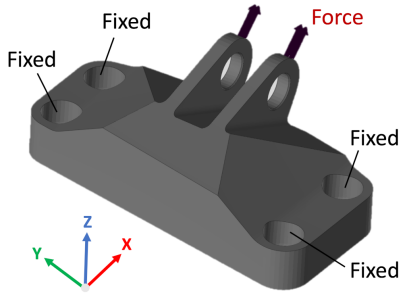


Figure 10: GE bracket loading condition.

Fig. 11 illustrates the optimized design at volume fraction of 0.3 with the milling tool approaching from different directions. Notice that with only one or two available tool orientations, large regions of the negative space would not be accessible for machining, hence the TO is not allowed to remove them during the iterations. As more orientations are included, the optimization has a larger feasible design space to explore. In every iteration, the IMF evaluates the minimum inaccessibility over a larger range of approach orientations. In this case, with all 6 coordinate axis-aligned directions at hand, the result of accessibility-constrained TO begins to resemble what one expects from unconstrained TO. Table 4 summarizes the results for the GE bracket example with a multi-axis milling tool.

As was discussed in Section 2, it is also possible to consider more geometrically complex tools while including fix-

turing devices in accessibility analysis. For instance, consider the 3-axis CNC milling setup of Fig. 12 where the tool assembly consists of the cutter, tool holder, and the clamping device. Fixturing includes 4 eye bolts that attach the bracket to the base plate via 4 holes that are also supposed to be retained throughout TO. Fig. 13 (a) shows the optimized design at a volume fraction of 0.5 alongside the non-machinable regions (in red). Fig. 13 (b) shows the optimized design at the same volume fraction with $w_{\text{acc}} = 0.5$ and $\lambda = 0.025$. In the presence of accessibility constraints, To takes a significantly different path in the design space to find the stiffest possible design (in a locally optimal sense) that can be manufactured with the given tool without colliding with the part or fixtures.

3.3. Quadcopter: 5-Axis Milling with 3-Point Grabber

In this section, let us consider the design of a quadcopter under hovering loading condition as shown in Fig. 14. The pocket at the center must be retained to mount battery and electronic boards. The material is Aluminum with $E = 70$ GPa and $\nu = 0.33$. Part resolution is about 300,000 voxels and target volume fraction is 0.20.

We aim to manufacture the optimized design with the 5-axis milling robot arm as illustrated in Fig. 16 where the raw stock is held by a 3-point grabber fixture. Figure 15 (a) shows the optimized design with no accessibility constraint imposed. The secluded volume ratio in this case is $V_{\Gamma_{\text{unc}}}/V_{\Omega_0} = 0.071$. Fig. 15 (b) shows the optimized design with accessibility constraint using $w_{\text{acc}} = 0.5$ and $\lambda = 0.025$, in which the secluded volume is zeroed out.

Fig. 17 shows volume of inaccessible regions at different volume fractions of optimized designs without considering the accessibility constraint. Fig. 18 shows the Pareto fronts of relative compliance and volume fraction for both unconstrained and constrained designs. At volume fraction of 0.20, the accessibility constraint results in an increase by a factor of 2.45 in the optimized compliance, i.e., $\frac{\varphi_{\text{con}}}{\varphi_{\text{unc}}} = 2.45$ to prevent inaccessible regions.

3.4. Support Bracket: 5-Axis Milling with Vise Fixture

Finally, let us consider the support bracket of Fig. 19. The material properties are those of Stainless Steel with $E = 270$ GPa and $\nu = 0.3$. The underlying discretization is about 200,000 hexahedral finite elements. The target volume fraction is 0.3. The optimized design is supposed

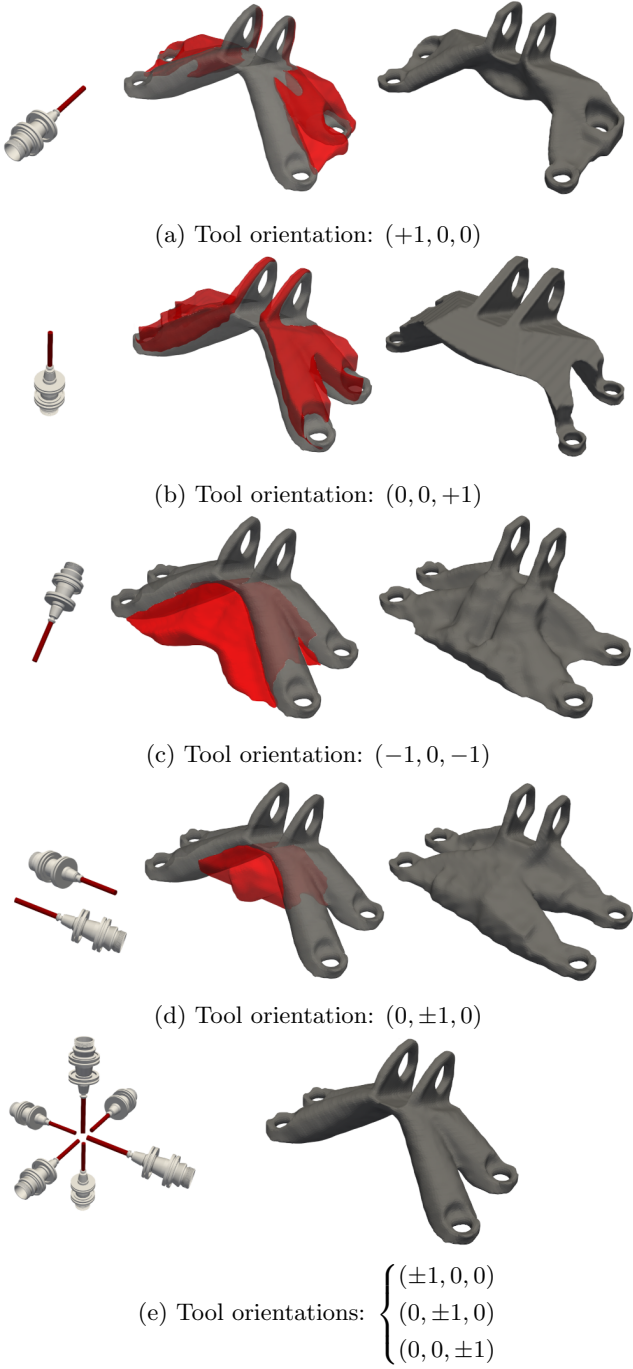


Figure 11: GE bracket at 0.3 volume fraction for multi-axis milling. The unconstrained and constrained TO parts in (e) are the same.

to be fabricated with the 5-axis milling robot arm and vise fixture as illustrated in Fig. 20. The highlighted components are modeled for computing IMF and rotation space is sampled at 10 orientations for the cutting tool. The discretized assembly of part and fixture used in convolution has a resolution of $196 \times 149 \times 97 \approx 1.8 \times 10^6$.

Fig. 21 illustrates the optimized designs for unconstrained and constrained cases. The secluded volume $V_{\Gamma_{\text{unc}}}$, i.e., volume of inaccessible regions outside the op-

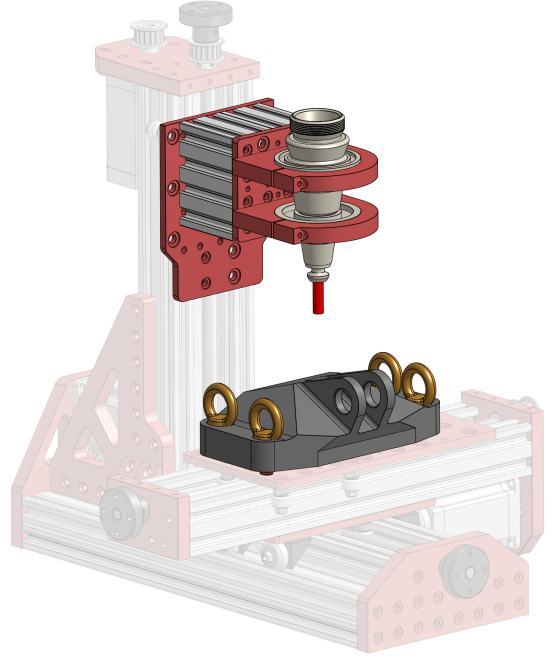
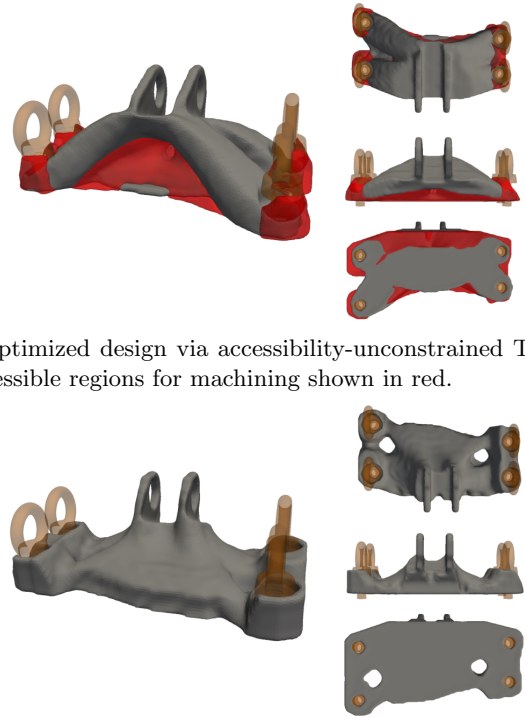


Figure 12: 3-axis milling setup for the GE bracket with eye-bolt fixtures. The tool assembly must avoid collisions with part and bolts.



(a) Optimized design via accessibility-unconstrained TO with inaccessible regions for machining shown in red.

(b) Optimized design via accessibility-constrained TO, machinable with specified tool and fixtures.

Figure 13: GE bracket at 0.5 volume fraction for 3-axis milling machine with fixtures.

timized design for the accessibility-unconstrained TO is about $0.18 V_{\Omega_0}$, which is significant. To impose the acces-

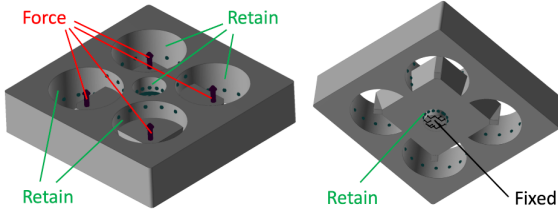
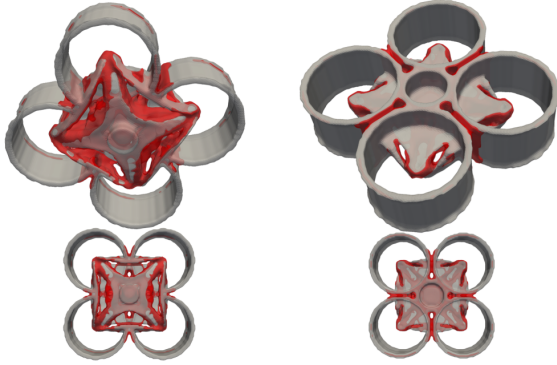
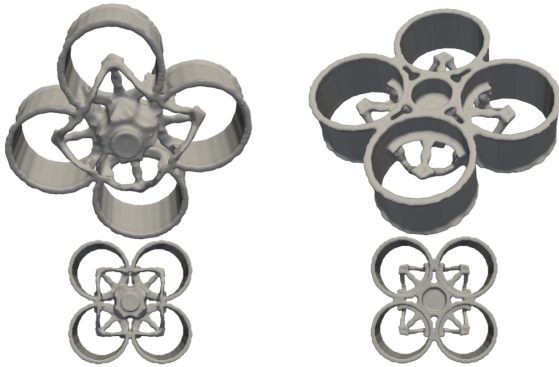


Figure 14: Quad-copter loading condition.



(a) Optimized design via accessibility-unconstrained TO with inaccessible regions for machining shown in red.



(b) Optimized design via accessibility-constrained TO, machinable with specified tool and fixtures.

Figure 15: Quadcopter at 0.2 volume fraction for 5-axis milling machine with 3-point grabber fixture and 10 sampled orientations.

sibility constraint, we begin with $w_{acc} = 0.1$ and gradually increase it to 0.5. In this example, the compliance of constrained and unconstrained designs are less than %1 different. In other words, our approach produces a machinable design with a negligible compromise in compliance.

3.4.1. Post-Processing: Machining Process Planning

It is important to note that the proposed TO framework *guarantees the existence of a machining process plan* with a given set of tool assemblies, orientations, and fixtures. Once TO comes up with a design, we employ a machining process planner to find a sequence of steps with which the negative space can be entirely removed in as few steps as possible. The simplest algorithm is based on a greedy criterion in terms of the maximal removable vol-

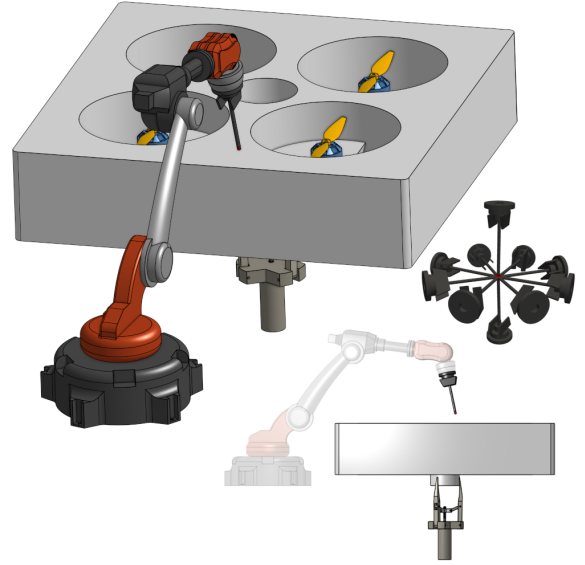


Figure 16: 5-axis milling setup for quadcopter design with 10 sampled orientations.

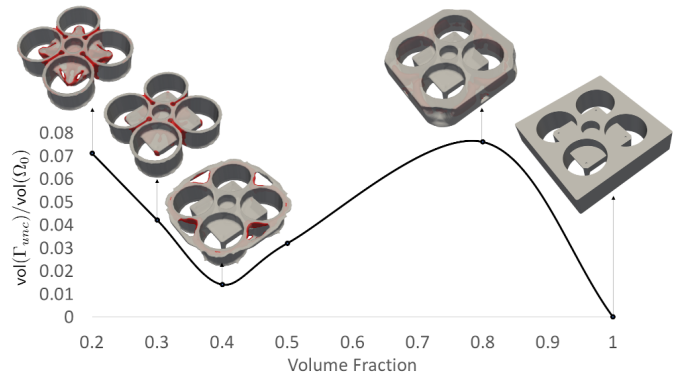


Figure 17: Inaccessible volume at different volume fractions for unconstrained quadcopter design.

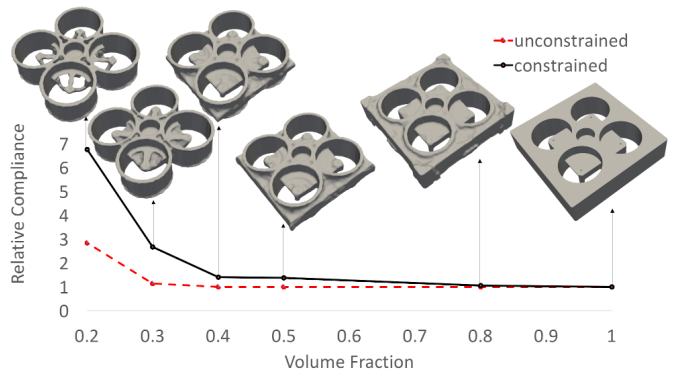


Figure 18: Relative compliance at different volume fractions for the quadcopter example.

umes. Starting from the initial design domain, at each step we select the oriented tool that can machine the largest volume compared to the others, and use it to remove the subset of the negative space that is accessible to this tool

at the specified orientation. We repeat this process until the entire negative space is removed. Figure 22 illustrates the 6-step machining process plan to produce the accessibility-constrained optimized design at 0.3 volume fraction, starting from the initial design domain.

More sophisticated combinatorial optimization algorithm and practical cost functions can be used to decide the optimal sequence of actions to be carried out by the given tools at the available orientations [51, 52]. In any case, having the upfront guarantee for manufacturability (i.e., existence of a process plan) and the proper set of tools and orientations is a significant assurance before proceeding to the costly task of process planning.

4. Conclusion

We presented a general approach to incorporating accessibility constraints for multi-axis machining into existing topology optimization (TO) methods for parts, tools, and fixtures of arbitrary shapes. We introduced the *inaccessibility measure field* (IMF) as a continuous field over

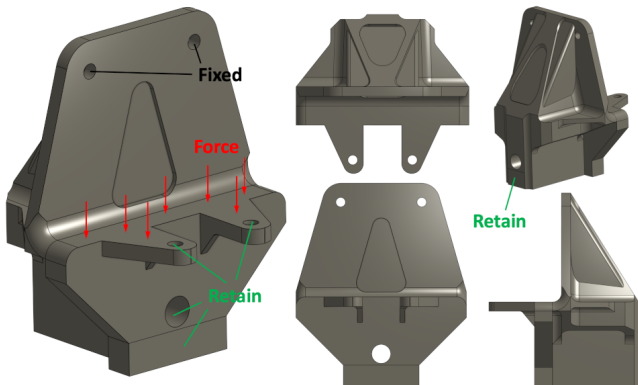
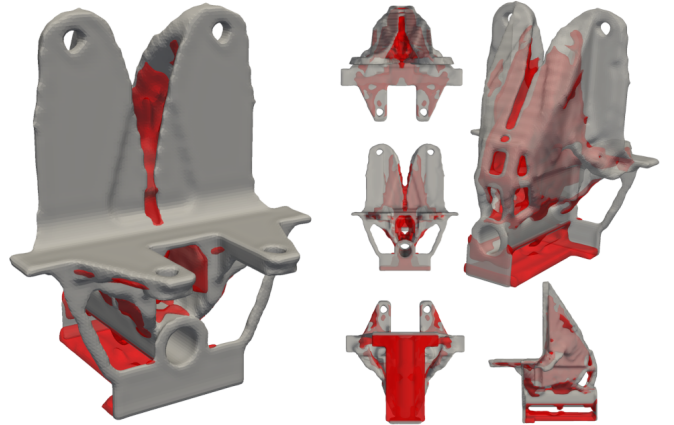


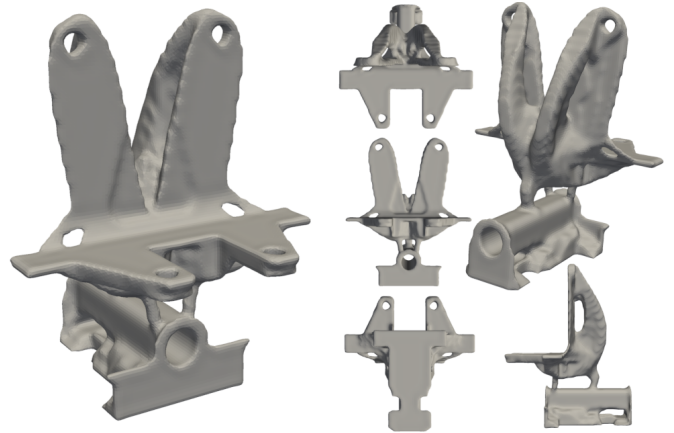
Figure 19: Support bracket geometry and loading condition.



Figure 20: Support bracket setup with 5-axis milling and vise fixture. The highlighted components are used in accessibility analysis. The robot is abstracted by its DOF for orientation sampling.



(a) Optimized design via accessibility-unconstrained TO with inaccessible regions for machining shown in red.



(b) Optimized design via accessibility-constrained TO, machinable with specified tool and fixtures.

Figure 21: Support bracket at 0.3 volume fraction for 5-axis milling machine with vise fixture and 10 sampled orientations.

the design domain to quantify the inaccessibility of different points in the part's negative space with respect to the geometry of intermediate design, tool assembly, fixtures, and available orientations. The IMF is expressed via well-established mathematical formalisms developed in spatial planning in terms of convolutions in configuration space. We project the convolutions back to the shape space by minimization over different candidate sharp points (on the cutter boundary) and sampled orientations, which guarantees a conservative approximation (i.e., over-estimation) and computational flexibility to balance the accuracy against time/memory budget. The methodology is fairly general and does not rely on artificial assumptions on geometric complexity of part, tool, or fixtures.

We extended the standard TO formulation to incorporate multi-axis machining constraints in order to reduce the discrepancy between as-designed and as-manufactured models. Specifically, we implemented the proposed algorithm as a density-based approach in both 2D and 3D. The effectiveness of the method was demonstrated through benchmark and realistic examples in 2D and 3D.

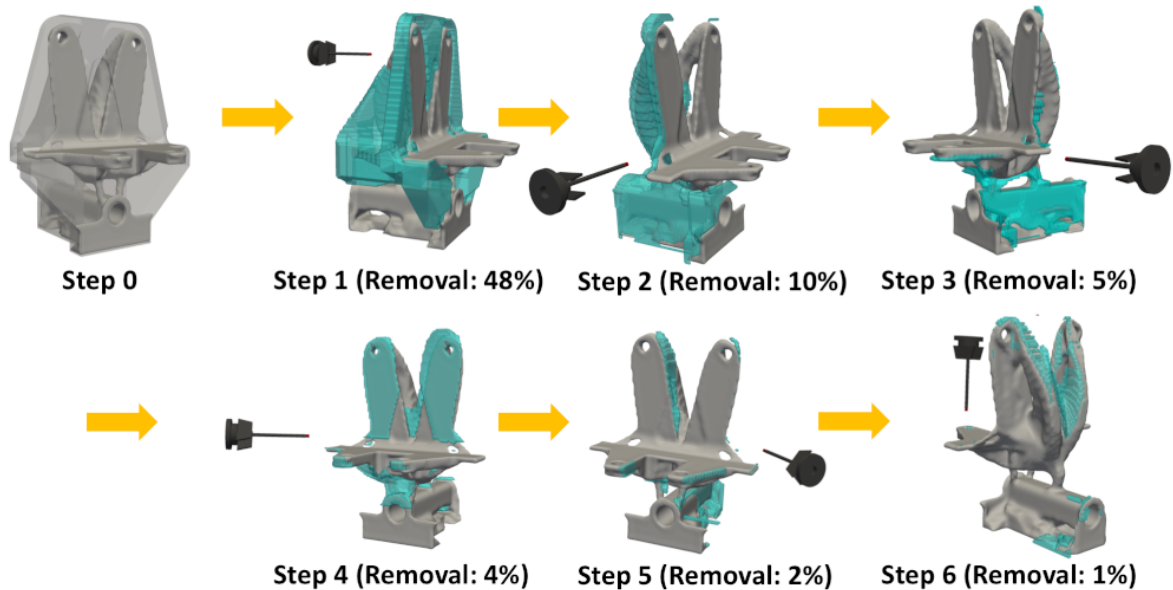


Figure 22: A 6-step machining plan based on maximum removable volume at every step.

Our formulation of accessibility constraint based on IMF guarantees that every point in the design’s negative space can be visited by at least one point on the cutter in at least one orientation without incurring a collision between the tool assembly, part, and fixtures. However, it is conceivable to encounter situations where a collision-free configuration is not accessible *in a continuous motion* from the rest configuration, i.e., the collision-free C-space is not path-connected. While this is limited to rare conditions (e.g., a small tool inside a large part cavity), the IMF can be corrected by artificially extending tool geometry via infinite half-spaces outside the bounding box (along the approach orientation) and correcting the convolution accordingly, or by invoking a motion planner such as Open Motion Planning Library (OMPL) [53]. The latter might be overkill for intermediate iterations within TO, but can be called for post-process validation.

Another limitation of our formulation is that accessibility and collision-avoidance do not fully capture machining constraints. In practice, different cutters are used for various machining operation such as milling slots, pockets, edges, large flat surfaces, and freeform shapes. Tolerance specs and surface quality are critical when machining functional interfaces. It is also important to consider physical constraints pertaining to the mechanics of the cutting process. While there are studies on these issues in the context of post-process manufacturability analysis and process planning, incorporating them in the TO design cycles is costly and requires further research.

Future work includes investigating the extension of the method to design for hybrid (i.e., interleaved AM/SM) sequences by developing IMF-like measures for printability and accessibility, over-deposition (or support structure) versus under-cut tradeoffs, and so forth.

Acknowledgement

This research was developed with funding from the Defense Advanced Research Projects Agency (DARPA). The views, opinions and/or findings expressed are those of the authors and should not be interpreted as representing the official views or policies of the Department of Defense or U.S. Government.

References

- [1] M. P. Bendsøe, M. Philip, O. Sigmund, *Topology Optimization—Theory, Methods, and Applications*, 2nd Edition, Springer-Verlag Berlin Heidelberg, 2009. doi:10.1007/978-3-662-05086-6.
- [2] O. Sigmund, K. Maute, *Topology optimization approaches, Structural and Multidisciplinary Optimization* 48 (6) (2013) 1031–1055. doi:10.1007/s00158-013-0978-6.
- [3] V. J. Challis, A. P. Roberts, J. F. Grotowski, L. C. Zhang, T. B. Sercombe, *Prototypes for bone implant scaffolds designed via topology optimization and manufactured by solid freeform fabrication, Advanced Engineering Materials* 12 (11) (2010) 1106–1110. doi:10.1002/adem.201000154.
- [4] L. Wang, P. K. Basu, J. P. Leiva, *Automobile body reinforcement by finite element optimization, Finite Elements in Analysis and Design* 40 (8) (2004) 879–893. doi:10.1016/S0168-874X(03)00118-5.
- [5] J. H. Zhu, W. H. Zhang, L. Xia, *Topology optimization in aircraft and aerospace structures design, Archives of Computational Methods in Engineering* 23 (4) (2016) 595–622. doi:10.1007/s11831-015-9151-2.
- [6] Z. Zhu, V. G. Dhokia, A. Nassehi, S. T. Newman, *A review of hybrid manufacturing processes—state of the art and future perspectives, International Journal of Computer Integrated Manufacturing* 26 (7) (2013) 596–615. doi:10.1080/0951192X.2012.749530.
- [7] K. A. Lorenz, J. B. Jones, D. I. Wimpenny, M. R. Jackson, *A review of hybrid manufacturing*, in: *Proceedings of the Solid Freeform Fabrication Conference*, Vol. 53, 2015, pp. 96–108.
- [8] J. M. Flynn, A. Shokrani, S. T. Newman, V. Dhokia, *Hybrid additive and subtractive machine tools—research and industrial de-*

- velopments, *International Journal of Machine Tools and Manufacture* 101 (2016) 79–101. doi:10.1016/j.ijmachtools.2015.11.007.
- [9] M. Merklein, D. Junker, A. Schaub, F. Neubauer, Hybrid additive manufacturing technologies—an analysis regarding potentials and applications, *Physics Procedia* 83 (2016) 549–559. doi:10.1016/j.phpro.2016.08.057.
- [10] T. Lozano-Perez, Spatial planning: A configuration space approach, *IEEE Transactions on Computers* C-32 (2) (1983) 108–120. doi:10.1109/TC.1983.1676196.
- [11] K. T. Zuo, L. P. Chen, Y.-Q. Zhang, J. Yang, Manufacturing and machining-based topology optimization, *The International Journal of Advanced Manufacturing Technology* 27 (5-6) (2006) 531–536. doi:10.1007/s00170-004-2210-8.
- [12] A. Sutradhar, J. Park, P. Haghghi, J. Kresslein, D. Detwiler, J. J. Shah, Incorporating manufacturing constraints in topology optimization methods: A survey, in: *International Design Engineering Technical Conferences and Computers and Information in Engineering Conference (IDETC/CIE'2017)*, American Society of Mechanical Engineers (ASME), 2017, pp. V001T02A073–V001T02A073. doi:10.1115/DETC2017-68192.
- [13] J. Liu, Y. Ma, A survey of manufacturing oriented topology optimization methods, *Advances in Engineering Software* 100 (2016) 161–175. doi:10.1016/j.advengsoft.2016.07.017.
- [14] J. Liu, A. T. Gaynor, S. Chen, Z. Kang, K. Suresh, A. Takezawa, L. Li, J. Kato, J. Tang, C. C. L. Wang, L. Cheng, X. Liang, A. C. To, Current and future trends in topology optimization for additive manufacturing, *Structural and Multidisciplinary Optimization* 57 (6) (2018) 2457–2483. doi:10.1007/s00158-018-1994-3.
- [15] M. Zhou, B. S. Lazarov, F. Wang, O. Sigmund, Minimum length scale in topology optimization by geometric constraints, *Computer Methods in Applied Mechanics and Engineering* 293 (2015) 266–282. doi:10.1016/j.cma.2015.05.003.
- [16] A. M. Mirzendehdel, K. Suresh, Support structure constrained topology optimization for additive manufacturing, *Computer-Aided Design* 81 (2016) 1–13. doi:10.1016/j.cad.2016.08.006.
- [17] M. Langelaar, Topology optimization of 3D self-supporting structures for additive manufacturing, *Additive Manufacturing* 12 (2016) 60–70. doi:10.1016/j.addma.2016.06.010.
- [18] X. Qian, Undercut and overhang angle control in topology optimization: A density gradient based integral approach, *International Journal for Numerical Methods in Engineering* 111 (3) (2017) 247–272. doi:10.1002/nme.5461.
- [19] A. M. Mirzendehdel, B. Rankouhi, K. Suresh, Strength-based topology optimization for anisotropic parts, *Additive Manufacturing* 19 (2018) 104–113. doi:10.1016/j.addma.2017.11.007.
- [20] G. Vantghem, V. Boel, W. De Corte, M. Steeman, Compliance, stress-based and multi-physics topology optimization for 3D-printed concrete structures, in: *RILEM International Conference on Concrete and Digital Fabrication*, Springer, 2018, pp. 323–332. doi:10.1007/978-3-319-99519-9_30.
- [21] M. Langelaar, Integrated component-support topology optimization for additive manufacturing with post-machining, *Rapid Prototyping Journal* 25 (2) (2019) 255–265. doi:10.1108/RPJ-12-2017-0246.
- [22] M. Zhou, R. Fleury, Y. K. Shyy, H. Thomas, J. Brennan, Progress in topology optimization with manufacturing constraints, in: *The 9th AIAA/ISSMO Symposium on Multidisciplinary Analysis and Optimization*, 2002, p. 5614. doi:10.2514/6.2002-5614.
- [23] Y. Wang, Z. Kang, Structural shape and topology optimization of cast parts using level set method, *International Journal for Numerical Methods in Engineering* 111 (13) (2017) 1252–1273. doi:10.1002/nme.5503.
- [24] J. K. Guest, M. Zhu, Casting and milling restrictions in topology optimization via projection-based algorithms, in: *ASME 2012 International Design Engineering Technical Conferences and Computers and Information in Engineering Conference (IDETC/CIE'2012)*, American Society of Mechanical Engineers (ASME), 2012, pp. 913–920. doi:10.1115/DETC2012-71507.
- [25] S. L. Vatanabe, T. N. Lippi, C. R. de Lima, G. H. Paulino, E. C. N. Silva, Topology optimization with manufacturing constraints: A unified projection-based approach, *Advances in Engineering Software* 100 (2016) 97–112. doi:10.1016/j.advengsoft.2016.07.002.
- [26] Q. Li, W. Chen, S. Liu, H. Fan, Topology optimization design of cast parts based on virtual temperature method, *Computer-Aided Design* 94 (2018) 28–40. doi:10.1016/j.cad.2017.08.002.
- [27] J. Liu, Y.-S. Ma, 3D level-set topology optimization: a machining feature-based approach, *Structural and Multidisciplinary Optimization* 52 (3) (2015) 563–582.
- [28] J. Liu, A. C. To, Topology optimization for hybrid additive-subtractive manufacturing, *Structural and Multidisciplinary Optimization* 55 (4) (2017) 1281–1299.
- [29] J. Liu, Y. Zheng, Y. Ma, A. Qureshi, R. Ahmad, A topology optimization method for hybrid subtractive-additive re-manufacturing, *International Journal of Precision Engineering and Manufacturing-Green Technology* (2019) 1–15doi:10.1007/s40684-019-00075-8.
- [30] J. A. Norato, B. K. Bell, D. A. Tortorelli, A geometry projection method for continuum-based topology optimization with discrete elements, *Computer Methods in Applied Mechanics and Engineering* 293 (2015) 306–327. doi:10.1016/j.cma.2015.05.005.
- [31] S. Zhang, J. A. Norato, A. L. Gain, N. Lyu, A geometry projection method for the topology optimization of plate structures, *Structural and Multidisciplinary Optimization* 54 (5) (2016) 1173–1190. doi:10.1007/s00158-016-1466-6.
- [32] M. Langelaar, Topology optimization for multi-axis machining, *Computer Methods in Applied Mechanics and Engineering* 351 (2019) 226–252. doi:10.1016/j.cma.2019.03.037.
- [33] J. C. Latombe, *Robot Motion Planning*, Vol. 124, Springer Science & Business Media, 2012.
- [34] T. C. Woo, B. F. Von Turkovich, Visibility map and its application to numerical control, *CIRP Annals-Manufacturing Technology* 39 (1) (1990) 451–454. doi:10.1016/S0007-8506(07)61094-4.
- [35] G. Elber, Accessibility in 5-axis milling environment, *Computer-Aided Design* 26 (11) (1994) 796–802. doi:10.1016/0010-4485(94)90093-0.
- [36] Z. Yin, H. Ding, Y. Xiong, Accessibility analysis in manufacturing processes using visibility cones, *Science in China Series E: Technological Sciences* 45 (1) (2002) 47–57. doi:10.1360/02ye9006.
- [37] A. Segall, J. Mizrahi, Y. J. Kim, G. Elber, Line accessibility of free form surfaces, *Graphical Models* 76 (5) (2014) 301–311. doi:10.1016/j.gmod.2014.03.014.
- [38] Y. J. Kim, G. Elber, M. Bartoñ, H. Pottmann, Precise gouging-free tool orientations for 5-axis CNC machining, *Computer-Aided Design* 58 (2015) 220–229. doi:10.1016/j.cad.2014.08.010.
- [39] B. Ezair, G. Elber, Automatic generation of globally assured collision free orientations for 5-axis ball-end tool-paths, *Computer-Aided Design* 102 (2018) 171–181. doi:10.1016/j.cad.2018.04.011.
- [40] B. van Sosin, M. Bartoñ, G. Elber, Accessibility for line-cutting in freeform surfaces, *Computer-Aided Design* 114 (2019) 202–214. doi:10.1016/j.cad.2019.05.014.
- [41] P. Bo, M. Bartoñ, On initialization of milling paths for 5-axis flank CNC machining of free-form surfaces with general milling tools, *Computer Aided Geometric Design* 71 (2019) 30–42. doi:10.1016/j.cagd.2019.04.012.
- [42] S. Nelaturi, M. Lysenko, V. Shapiro, Rapid mapping and exploration of configuration space, *Journal of Computing and Information Science in Engineering* 12 (2) (2012) 021007. doi:10.1115/1.4005776.
- [43] M. Lysenko, S. Nelaturi, V. Shapiro, Group morphology with convolution algebras, in: *Proceedings of the 14th ACM Symposium on Solid and Physical Modeling (SPM'2010)*, Association of Computing Machinery (ACM), 2010, pp. 11–22. doi:

- 10.1145/1839778.1839781.
- [44] L. E. Kavragi, Computation of configuration-space obstacles using the fast Fourier transform, *IEEE Transactions on Robotics and Automation* 11 (3) (1995) 408–413. doi:10.1109/70.388783.
- [45] A. M. Mirzendehtdel, M. Behandish, S. Nelaturi, Exploring feasible design spaces for heterogeneous constraints, *Computer-Aided Design* 115 (2019) 323–347. doi:10.1016/j.cad.2019.06.005.
- [46] K. Suresh, A 199-line Matlab code for Pareto-optimal tracing in topology optimization, *Structural and Multidisciplinary Optimization* 42 (5) (2010) 665–679. doi:10.1007/s00158-010-0534-6.
- [47] R. B. Tilove, A. A. G. Requicha, Closure of Boolean operations on geometric entities, *Computer-Aided Design* 12 (5) (1980) 219–220. doi:10.1016/0010-4485(80)90025-1.
- [48] M. Behandish, Analytic methods for geometric modeling, Ph.D. dissertation, University of Connecticut (2017). URL <https://opencommons.uconn.edu/dissertations/1400/>
- [49] O. Sigmund, A 99 line topology optimization code written in matlab, *Structural and multidisciplinary optimization* 21 (2) (2001) 120–127.
- [50] E. Andreassen, A. Clausen, M. Schevenels, B. S. Lazarov, O. Sigmund, Efficient topology optimization in Matlab using 88 lines of code, *Structural and Multidisciplinary Optimization* 43 (1) (2011) 1–16. doi:10.1007/s00158-010-0594-7.
- [51] S. Nelaturi, G. Burton, C. Fritz, T. Kurtoglu, Automatic spatial planning for machining operations, in: 2015 IEEE International Conference on Automation Science and Engineering (CASE), Institute of Electrical and Electronics Engineers (IEEE), 2015, pp. 677–682. doi:10.1109/CoASE.2015.7294158.
- [52] M. Behandish, S. Nelaturi, J. de Kleer, Automated process planning for hybrid manufacturing, *Computer-Aided Design* 102 (2018) 115–127, special Issue on the 22nd ACM Symposium on Solid and Physical Modeling (SPM’2018). doi:10.1016/j.cad.2018.04.022.
- [53] I. A. Şucan, M. Moll, L. E. Kavragi, The Open Motion Planning Library, *IEEE Robotics & Automation Magazine* 19 (4) (2012) 72–82, <http://ompl.kavrakilab.org>. doi:10.1109/MRA.2012.2205651.
- [54] L. Ma, R. D. Chamberlain, K. Agrawal, Analysis of classic algorithms on GPUs, in: 2014 International Conference on High Performance Computing & Simulation (HPCS), Institute of Electrical and Electronics Engineers (IEEE), 2014, pp. 65–73. doi:10.1109/HPCSim.2014.6903670.

Appendix A. Morphology via Convolutions

Here we explain in intuitive terms how the morphological concepts of C -space obstacles and sweeps, used in Section 2.1.1 to define accessible regions, can be defined implicitly and computed by convolutions.

First, let us consider the first convolution in (8) that implicitly defines the set of colliding translations $D \subseteq \mathbb{R}^3$ for a fixed rotation $R \in \text{SO}(3)$. This convolution is defined as an integral over the shape space (i.e., where the design resides) with a free variable in the translation space:

$$(\mathbf{1}_O * \tilde{\mathbf{1}}_{RT})(\mathbf{t}) = \int_{\mathbb{R}^3} \mathbf{1}_O(\mathbf{x}) \tilde{\mathbf{1}}_{RT}(\mathbf{t} - \mathbf{x}) dv[\mathbf{x}], \quad (\text{A.1})$$

The integral is nonzero iff the integrand becomes nonzero over a region of nonzero volume, meaning that both indicator functions, one of which is shifted to apply a relative translation $\mathbf{t} \in \mathbb{R}^3$, are nonzero. This implies a volumetric interference between O and $(R, \mathbf{t})T$, noting that

$\mathbf{1}_{(R, \mathbf{t})T}(\mathbf{x}) = \mathbf{1}_{RT+\mathbf{t}}(\mathbf{x}) = \mathbf{1}_{RT}(\mathbf{x} - \mathbf{t}) = \mathbf{1}_{-RT}(\mathbf{t} - \mathbf{x})$. The reflection $RT \rightarrow -RT$ after rotation is to flip the shifted argument $(\mathbf{x} - \mathbf{t}) \rightarrow (\mathbf{t} - \mathbf{x})$ to match the standard definition for convolutions. $dv[\mathbf{x}] = dx_1 dx_2 dx_3$ for $\mathbf{x} = (x_1, x_2, x_3)$ is the volume element in the shape space.

The second convolution in (9) that implicitly defines the sweep of cutter along the collision-free motion can be expressed as a similar integral, this time over the translation space, with a free variable over the shape space:

$$(-\mathbf{1}_D * \mathbf{1}_{RK})(\mathbf{x}) = \int_{\mathbb{R}^3} -\mathbf{1}_D(\mathbf{t}) \mathbf{1}_{RK}(\mathbf{x} - \mathbf{t}) dv[\mathbf{t}], \quad (\text{A.2})$$

noting that $\mathbf{1}_{D^c}(\mathbf{t}) = -\mathbf{1}_D(\mathbf{t})$ is nonzero for collision-free translations $\mathbf{t} \in D^c$ and $\mathbf{1}_{(R, \mathbf{t})K}(\mathbf{x}) = \mathbf{1}_{RK+\mathbf{t}}(\mathbf{x}) = \mathbf{1}_{RK}(\mathbf{x} - \mathbf{t})$ is nonzero if the query point $\mathbf{x} \in \mathbb{R}^3$ is visited by the transformed cutter $(R, \mathbf{t})K$, respectively. The convolution is nonzero if the query point is inside the sweep $A(O, T, K)$, and the converse is true if the motion has no singularities,⁵ as expected under quite general conditions. $dv[\mathbf{t}] = dt_1 dt_2 dt_3$ for $\mathbf{t} = (t_1, t_2, t_3)$ is the volume element, this time in the translation space.

Note that we use the sign functions in (8) and (9) because indicator functions are not closed under convolutions [48]. However, for TO penalization, we do not need binary indicator functions as we do for morphological applications. The output of (A.1) can be directly used not only to *classify* configurations against the C -obstacle as in/out (as in indicator functions) but also to *quantify* them in terms of a continuous measure of collision. We need is to project this measure back to the shape space using the proper operator that combines the collision measure for different configurations that bring different candidate sharp points to the same point in the shape space.

Intuitively, the output of (A.2) quantifies accessibility by a summation (i.e., implicit set union) over different ways the sweep might pass through the query point, i.e., different ways by which the sharp points can touch the query point for machining. However, it does *not* quantify inaccessibility, as it returns zero for all inaccessible points. An alternative approach for implicitization of set union/intersection is via max/min operations. In this paper, we apply a minimum (i.e., implicit intersection) to the output of (A.1) over different choices of sharp points, instead of using (A.2), to quantify inaccessibility, which led to the definition of IMF in (13) of Section 2.1.3.

Appendix B. Complexity Analysis

For a voxelized representation of the design (as used in TO), fixtures, and tool assembly, the convolution can be computed rapidly using FFTs [44], and parallelized on multi-core CPUs/GPUs. Using the same Cartesian grid

⁵If the motion has lower-dimensional features, they will be regularized as the volumetric integral cannot capture sweeps along curves or surfaces [48].

for shape voxelization and translational motion digitization with a grid size of $n_G \gg 1$, each convolution takes two forward FFTs, a pointwise multiplication in frequency domain, and one inverse FFT with time complexity of $2O(n_G \log n_G) + O(n_G) + O(n_G \log n_G) = O(n_G \log n_G)$.

For $n_R \geq 1$ sampled rotations, it takes $O(n_R n_G \log n_G)$ time to compute all convolution fields, stacked together to form a single group convolution field in the \mathbb{C} -space.

For $n_K \geq 1$ sharp points, the convolution field for each rotation is queried at different translations $\mathbf{t} = (\mathbf{x} - R\mathbf{k})$, i.e., within a \mathbb{C} -space neighborhood $\mathfrak{N}(\mathbf{x}; R) := (\mathbf{x} - RK)$ that resembles a reflected and rotated image of the cutter. It takes an additional $O(n_K)$ steps to perform these queries for every oriented tool and compute the minimum, without the need for re-computing the convolution for different shifts. Hence the total time complexity for computing IMF for a single tool assembly is $O(n_R n_G \log n_G) + O(n_R n_K) = O(n_R (n_G \log n_G + n_K))$.

Finally, given $n_T \geq 1$ available tool assemblies, computing the IMF takes $O(n_T n_R (n_G \log n_G + n_K))$ steps. Theoretically, as long as $n_K = O(n_G \log n_G)$, the sequential time complexity is $O(n_T n_R n_G \log n_G)$. We achieve near-linear speed-up by distributing the work on multi-core CPUs/GPUs, but the precise complexity analysis depends on the GPU architecture [54]. If we use the same resolution to resolve the cutter as the grid size for convolution, then $n_K \ll n_G$ since the cutter is typically much smaller in size than the design domain. Even if we down-sample the sharp points to one or a few representative points on the boundary (i.e., $n_K = O(1)$) the approximate IMF captures most of the qualitative features of the exact IMF, as we showed for simple 2D examples in [45].

Our results show that the main bottleneck in TO iterations is the FEA. The IMF computation using FFT-based convolution on the GPU outperforms FEA by an order of magnitude for $n_G \approx 10^5$ voxels and the discrepancy grows with the problem size (see Table 3 of Section 3). The main challenge with computing IMF is memory, as we need to store convolution fields for all tool assemblies and their re-sampled grid interpolation at different orientations. The space complexity is $O(n_T n_R n_G)$ if all of them are retained for rapid querying, which can be prohibitive for high-resolution parts in large-scale TO. Given a fixed memory budget of $O(n_M)$, we serialize the parallel computations at a small time cost as follows. We store a batch of $O(n_M/n_G)$ convolution fields at-a-time, each computed on the GPU as a 3D array of size $O(n_G)$. We arrange their shifted copies for different sharp points into a 4D array of size $O(n_M)$. We compute and store the partial minimum field by pointwise comparison on the GPU, discard the 4D array, and move on to comparing the next batch with the partial minimum until we cover all of them.